Solubilities and Self-Diffusion Coefficients of Light n-Alkanes in NaCl Solutions at the Temperature Range (278.15-308.15) K and Pressure Range (1-300) bar and Thermodynamics Properties of Their Corresponding Hydrates at (150-290) K and (1-7000) bar

Fang, Bin; Habibi, Parsa; Moultos, Othonas A.; Lü, Tao; Ning, Fulong; Vlugt, Thijs J.H.

DOI
10.1021/acs.jced.3c00225

Publication date
2024

Document Version
Final published version

Published in
Journal of Chemical and Engineering Data

Citation (APA)
Fang, B., Habibi, P., Moultos, O. A., Lü, T., Ning, F., & Vlugt, T. J. H. (2024). Solubilities and Self-Diffusion Coefficients of Light n-Alkanes in NaCl Solutions at the Temperature Range (278.15-308.15) K and Pressure Range (1-300) bar and Thermodynamics Properties of Their Corresponding Hydrates at (150-290) K and (1-7000) bar. *Journal of Chemical and Engineering Data*, *69*(10), 3330-3346. https://doi.org/10.1021/acs.jced.3c00225

Journal of Chemical&Engineering Data

Editors' Choice

Open Access

pubs.acs.org/jced

Article

Solubilities and Self-Diffusion Coefficients of Light *n*-Alkanes in NaCl Solutions at the Temperature Range (278.15−308.15) K and Pressure Range (1−300) bar and Thermodynamics Properties of Their Corresponding Hydrates at (150−290) K and (1−7000) bar

Bin Fang, Parsa Habibi, Othonas A. Moultos,* Tao Lü, Fulong Ning, and Thijs J. H. Vlugt*

Cite This: *J. Chem. Eng. Data* 2024, 69, 3330−3346

Read Online

ACCESS | Metrics & More | Article Recommendations | Supporting Information

ABSTRACT: Continuous Fractional Component Monte Carlo (CFCMC) and molecular dynamics (MD) simulations are performed to calculate the solubilities and self-diffusion coefficients of four light *n*-alkanes (methane, ethane, propane, and *n*-butane) in aqueous NaCl solutions as well as the thermodynamic properties of their corresponding hydrate crystals. Correction factors k_{ij} to the Lorentz−Berthelot combining rules for alkane groups (CH_3) and water are optimized (k_{ij} = 1.04) by fitting excess chemical potentials to experimental data at 1 bar and 298.15 K. Using these values of k_{ij}, we calculate the solubilities of the four alkanes in aqueous NaCl solutions with different molalities (0−6) mol/kg at different temperatures (278.15−308.15) K and pressures (1, 100, 200, 300) bar. The diffusion coefficients of the four alkanes in NaCl solutions (0−6) mol/kg are calculated at different temperatures (278.15−308.15) K and 1 bar and corrected for the finite-size effects. The lattice parameters of the corresponding hydrates with different guest molecules are computed using MD simulations at different temperatures (150−290) K and pressures (5−700) MPa. Isothermal compressibilities at 287.15 K and thermal expansion coefficients at 14.5 MPa for the corresponding hydrates are calculated. We present an extensive collection of thermodynamic data related to gas hydrates that contribute to a fundamental understanding of natural gas hydrate science.

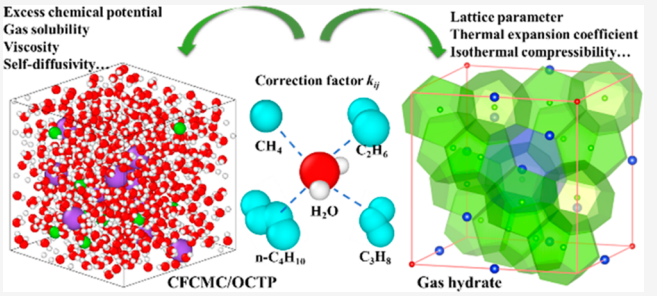

1. INTRODUCTION

Natural gas hydrates (NGHs) are ice-like crystallization compounds, in which natural gas (mainly composed of light *n*-alkanes such as methane, ethane, propane, and *n*-butane) is trapped in polyhedral cages formed by hydrogen-bonded (H-bonded) water molecules at specific pressure and temperature conditions.[1] There are three typically identified hydrate structures on earth, and the formation of crystals mainly depends on the size of the guest molecule.[1] Hydrates usually occur on marine sediments and permafrost regions[1] and in pipelines.[2] The global energy content in gas hydrates is conservatively estimated to be twice that of all other fuel sources together; thus, NGHs are considered as alternative energy resources.[3] Moreover, hydrates have significant potential for water, energy, and environmental industrial applications, including CO_2 capture and sequestration (CCS),[4] hydrogen storage,[5] seawater desalination,[6] wastewater treatment,[7] and gas transport.[8] The exploitation and application of hydrates are based on accurate information about the phase change kinetics (i.e., formation and dissociation) and thermodynamic properties of NGHs that have been extensively explored. Two physical parameters that are very important for controlling the hydrate phase change are the solubilities and self-diffusion coefficients of light alkanes in water,[9] and particularly in NaCl solutions,[10] as hydrates often occur in seabed sediments.[1]

To date, many experimentalists have measured the solubility of methane,[11−17] ethane,[11,17] propane,[12,18−21] and butane[16] in pure water and in NaCl solutions[22−28] at different temperatures, pressures, and molalities. Wilhelm et al.[29] presented a review on the solubility of gases in pure water at normal pressure. In NaCl solutions, the solubility of alkanes decreases as the molality (mol salt/kg water) of the salt increases. This phenomenon is commonly referred to as the "salting out effect".[30] However, the data obtained from experimental measurements are still insufficient, and the majority of the studies conducted has focused on methane. For the prediction of gas solubility in solutions, equation of state (EoS) based models are often used, such as GCNLF EoS,[31] GC EoS,[32] and SAFT-based EoS.[33] EoS models may not accurately describe gas solubility in complex

Special Issue: In Honor of Maria Eugenia Macedo

Received: April 10, 2023
Accepted: June 20, 2023
Published: July 11, 2023

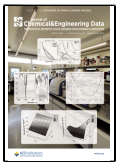

systems and often neglect the interaction between the gas and liquid phases, resulting in potential errors in gas solubility calculations. Force field-based Monte Carlo (MC) simulations[34−36] can effectively overcome this problem and are well-suited for estimating thermodynamic properties, such as excess chemical potentials and gas solubilities. Docherty et al.[34] introduced a positive deviation in the energetic Lorentz−Berthelot rule to correct the interactions between methane and water and calculated the excess chemical potential of gas in water and the properties of methane hydrates. Additionally, machine learning has also been used to predict the solubilities of light alkanes in pure water and aqueous electrolyte solutions.[37] To discuss the salting out effects of alkanes in aqueous electrolyte solutions,[38] the Setschenow relation is often used[39]

$$\ln\left(\frac{\chi^0_{\text{alkane}}}{\chi_{\text{alkane}}}\right) = k_{\text{salt}} m_{\text{salt}} \quad (1)$$

where χ^0_{alkane} and χ_{alkane} represent the mole fractions of alkane in pure water and electrolyte solutions, respectively, m_{salt} denotes the molality of salt (mol salt/kg water), and k_{salt} is the Setschenow salting out constant. The Setschenow constants usually decrease with temperature and depend on the nature of the gas.[40] Within a small temperature range, the variation in the Setschenow constants with temperature can be ignored.[24]

The mass transport of light alkanes in water and an electrolyte system plays an important role in the formation and dissociation kinetics processes of hydrates, especially for the phase change rate.[41,42] The self-diffusion coefficients of methane, ethane, propane, and *n*-butane have been measured in water[43−45] and in aqueous electrolyte systems.[46] Molecular dynamics (MD) simulations are widely used to calculate diffusion coefficients of pure compounds in mixtures. Pokharel et al.[47] calculated the self-diffusion coefficients of methane, ethane, propane, and *n*-butane in water using MD simulations. Chen et al.[46] calculated the diffusion coefficients of methane in water/brine (3.5 wt % NaCl solution). Yeh and Hummer[48,49] discovered that the computed self-diffusion coefficients in MD simulations are strongly influenced by the system size. To correct the systematic errors, these authors developed a hydrodynamics-based finite-size correction term for classical MD simulations to adjust the self-diffusion coefficients.

Comprehending thermodynamic properties, including thermal expansion coefficients and isothermal compressibilities, is crucial for hydrate exploitation. The thermal expansion coefficient of hydrates is fundamental information for risk assessment studies concerning the mechanical stability of hydrate-bearing earth sediments.[50] The detection of natural gas hydrates (NGHs) in sediments is typically performed using the propagation of seismic waves, which depends on the elastic properties (compressibility) of the medium.[51] Hester et al.[52] measured the hydrate lattice parameters for both sI and sII hydrates as a function of temperature and estimated the thermal expansion coefficient of different hydrates. Manakov et al.[53] presented experimental data of the lattice parameters for gas hydrates as a function of pressure (0−3) GPa and obtained the gas hydrate bulk modulus. To date, many experimental results have been reported for the thermal expansion coefficient[54−60] and compressibility[61−65] of gas hydrates. In addition, MD simulations have proven to be a valuable tool for determining the thermodynamic properties of gas hydrates for a broad temperature and pressure range, helping to explain the variations in thermodynamic properties between hydrate systems containing different guest molecules.[66,67]

Several experimental and simulation studies have been conducted for obtaining the solubilities and transport properties of alkanes in pure water and aqueous NaCl solutions. These data are for limited temperature/pressure ranges; such data at hydrate formation conditions, and particularly for NaCl solutions data, are largely lacking. The remainder of this study is structured as follows. In Section 2, we first show the force field, explain how to calculate solubilities and self-diffusion coefficients, and build hydrate crystals with different guest molecules to calculate thermodynamics properties using classical MC and MD simulations. In Section 3, we introduce a correction factor k_{ij} between alkane groups (CH_3) and water by calculating the excess chemical potential at 298.15 K and 1 bar. Using this correction factor, we calculated the solubilities and diffusion coefficients of the four alkanes in NaCl solutions at temperatures ranging from 278.15 to 308 K, pressures ranging from 1 to 300 bar, and molalities ranging from 0 to 6 mol/kg. We also calculated the compressibility and expansion coefficients for the four corresponding hydrates. Finally, Section 4 summarizes the conclusions drawn from the study.

2. METHODS

2.1. Force Fields. Water is modeled using the TIP4P/2005 force field.[68] This model predicts the densities, viscosities, and self-diffusion coefficients of water with high accuracy over a wide temperature range and performs well in an aqueous salt solution system containing gases.[34,36] The description of the CH_4 molecule and its interaction with water are handled in the same way as in Docherty's study.[34] The TraPPE-UA force field[69] is used for the other three light alkane molecules i.e., C_2H_6, C_3H_8, and n-C_4H_{10}. The Madrid-2019 force field proposed by Zeron et al.[70] is used for Na^+ and Cl^- with scaled changes, which considers the polarization effect and improves the description of the salt system in water. All force field details are provided in Table S1, Table S2, and Table S3 in the Supporting Information.

Table 1. Description of All the Species Used in the Simulations

Chemical name	Chemical formula	CAS number	Force field
Water	H_2O	7732-18-5	TIP4P/2005[68]
Methane	CH_4	74-82-8	Hirschfelder[34]
Ethane	C_2H_6	74-84-0	TraPPE[69]
Propane	C_3H_8	74-98-6	TraPPE[69]
Butane	C_4H_{10}	106-97-8	TraPPE[69]
Sodium ion	Na^+	7440-23-5	Madrid-2019[70]
Chlorine ion	Cl^-	16887-00-6	Madrid-2019[70]

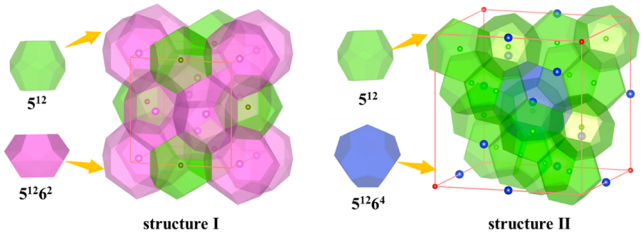

Figure 1. Host structures of sI and sII unit hydrate cells: 5^{12} cages colored in green, $5^{12}6^2$ cages colored in purple, and $5^{12}6^4$ cages presented in blue.

https://doi.org/10.1021/acs.jced.3c00225
J. Chem. Eng. Data 2024, 69, 3330−3346

The chemical formulas, CAS numbers, and force fields of all species used in the simulations are listed in Table 1. The nonbonded intermolecular interactions are handled by Lennard-Jones (LJ) and Coulombic potentials, which are expressed as follows[71]

$$U(r_{ij}) = U^{LJ} + U^{C} = 4\varepsilon_{ij}\left[\left(\frac{\sigma_{ij}}{r_{ij}}\right)^{12} - \left(\frac{\sigma_{ij}}{r_{ij}}\right)^{6}\right] + \frac{q_i q_j}{4\pi\varepsilon_0 r_{ij}} \quad (2)$$

where r_{ij} is the distance between particles i and j, ε_{ij} is the depth of the LJ potential well, and σ_{ij} is the distance at which the pair potential energy U is zero. An unshifted potential (+tail corrections) was used so that the force field used in both the MC and MD simulations was identical. The energy (ε_{ij}) and distance (σ_{ij}) parameters for the cross interaction between the groups in the alkanes and water were described by the modified version of the Lorentz−Berthelot combining rules (a correction factor k_{ij} is applied to adjust the energetic cross interactions (ε_{ij})):[72]

$$\begin{cases} \sigma_{ij} = \dfrac{\sigma_{ii} + \sigma_{jj}}{2} \\ \varepsilon_{ij} = k_{ij}\sqrt{\varepsilon_{ii}\varepsilon_{jj}} \end{cases} \quad (3)$$

Deviations from this rule can be accounted for by using values of k_{ij} that differ from 1. For the energetic cross interactions between alkane groups and ions, as well as between water and ions, the value of k_{ij} in eq 3 is set to 1, which corresponds to the conventional Lorentz−Berthelot combining rule.

2.2. Monte Carlo Simulations. The Continuous Fractional Component Monte Carlo (CFCMC) technique in the NPT ensemble is used to calculate the excess chemical potentials and solubilities of the four light alkanes in aqueous NaCl solutions. All MC simulations are performed by the open-source Brick-CFCMC software.[73−75] A so-called fractional molecule of each component type was introduced into the simulation. All of the MC simulation systems contained both water and ion molecules. The total number of water molecules in each system is fixed at 270, while the number of ions is determined by the NaCl molality present in the solution. An expanded conventional NPT ensemble was used to control the pressure and temperature. The interaction potential for the fractional molecule is determined by the fractional parameter $\lambda \in [0,1]$. When λ is equal to zero, no interactions between the fractional molecules and surrounding molecules are present (i.e., the fractional molecule acts as an ideal gas molecule). When λ is equal to one, this fractional molecule acts as a "whole molecule" (i.e., full interaction between the fractional molecule and surrounding molecules). The excess chemical potential of alkanes in aqueous NaCl solutions can be calculated from the probability distribution of λ[76]

$$\mu_{ex} = -k_B T \ln\left(\frac{p(\lambda = 1)}{p(\lambda = 0)}\right) \quad (4)$$

where μ_{ex} is the excess chemical potential with respect to ideal gas, T is the temperature, and $p(\lambda = 0)$ and $p(\lambda = 1)$ are the probabilities when λ equals 0 and 1, respectively.

The Henry coefficient K_H can be computed from[39]

$$K_H = \frac{k_B T(N_{H_2O} + N_{salt})}{V} \exp(\mu_{ex}/k_B T) \quad (5)$$

where N_{H_2O} and N_{salt} are the molecular number of water and salt, respectively, and V is the volume of the system. At low pressure, the concentration of the solute in a dilute solution is directly proportional to its mole fraction (x). This relationship is described by Henry's law, which can be expressed as follows:

$$P = K_H \cdot x \quad (6)$$

At high pressures, the solubility of light alkanes is computed by using the Gibbs Ensemble, where a fractional molecule is used for the insertion and deletion of light alkane molecules. The fugacity coefficients for the light alkanes at different temperatures and pressure conditions are computed using REFPROP software.[77] Table S4 in the Supporting Information contains a list of all fugacity coefficients.

During MC simulations, both Lennard-Jones and Coulombic interactions were cut off at 9 Å, and analytical tail corrections are implemented. The Ewald method was used to calculate the long-range electrostatic interaction energy.[78] The probabilities of selecting trial moves were as follows: 34% translations, 24% rotations, and 10% changes in the geometry of molecules (angle and dihedral), 20% changes in the fractional parameter, and 2% volume changes, 1×10^4 cycles to initialize the system, 5×10^5 cycles were performed for system equilibration, and 1×10^6 cycles were performed for production in the simulations. A cycle is defined as a set of N trial moves. For excess chemical potential calculations, the simulation temperature range is 278.15−308.15 K, and the pressure is 1 bar. For solubility calculations, the simulation temperatures range is 278.15−308.15 K, and the pressure is 1−300 bar.

2.3. Molecular Dynamics Simulations. MD simulations are carried out using the large-scale atomic/molecular massively parallel simulator (LAMMPS) to calculate the transport properties of light *n*-alkanes in aqueous NaCl solutions and the thermodynamic properties of their corresponding gas hydrates. To simulate the transport properties, the initial MD systems consist of *n*-alkane, water, and ion molecules. In each system, there is only one *n*-alkane molecule and 555 water molecules, and the number of ions is determined by NaCl molality. The initial step in simulating the thermodynamic properties involves creating a molecular-level crystal structure of the corresponding alkane hydrate. Based on experimental results, methane and ethane hydrates are often present in the sI structure, whereas propane and *n*-butane hydrates are in the sII structure. It should be noted that the formation of *n*-butane hydrates requires a "help gas" (e.g., CH_4);[79,80] therefore, we calculated the thermodynamic properties of a butane+methane binary hydrate. The coordinates of the host water molecules in both crystal structures are determined by Takeuchi's work,[81] in which the oxygen atom positions of the hydrate are determined by XRD results,[82] and the hydrogen orientation in water molecules is adjusted to adhere to the Bernal-Fowler rule and minimize both the structural potential energy and dipole moment. Host structures of sI and sII unit hydrate cells are shown in Figure 1. Methane and ethane molecules fully occupy the 5^{12} and $5^{12}6^2$ cages in the sI structure of hydrate. Propane and butane molecules are located in the center of the large $5^{12}6^4$ cage, and the "help gas" CH_4 occupies the 5^{12} cages in the sII structure of the hydrate. The initial MD configurations of methane and ethane hydrates are in a $3 \times 3 \times 3$ supercell with a 12.03 Å lattice parameter for an sI unit cell.[81] The propane and

https://doi.org/10.1021/acs.jced.3c00225
J. Chem. Eng. Data 2024, 69, 3330−3346

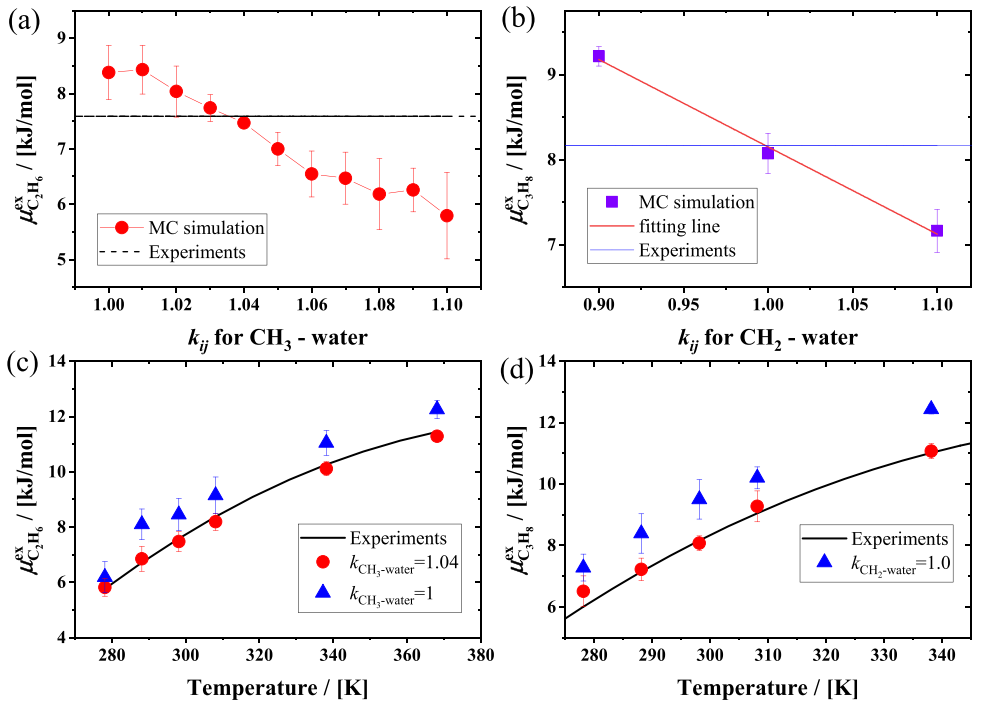

Figure 2. Comparison of simulated and experimental excess chemical potentials of ethane (a) and propane (b) in water by changing the LJ k_{ij} parameter of the CH_3 (a) and CH_2 (b) groups and water molecules at 298.15 K and 1 bar. The excess chemical potential of ethane (c) and propane (d) in water as a function of temperature at 1 bar by MC simulation using different scaling k_{ij} parameters and the experimental results.[29]

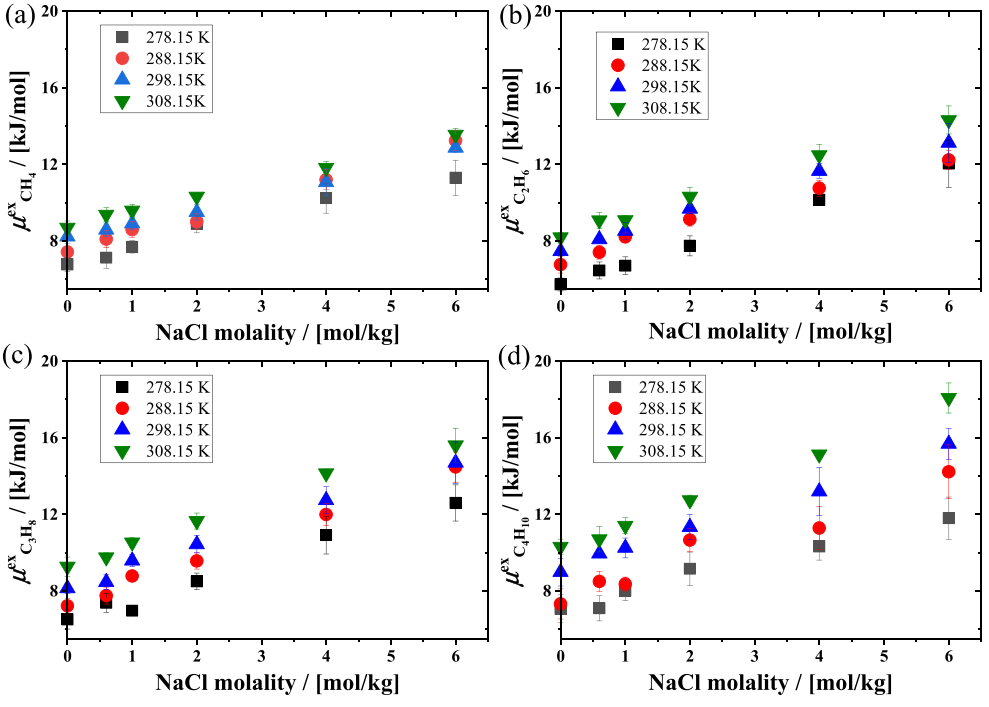

Figure 3. Excess chemical potentials of (a) methane, (b) ethane, (c) propane, and (d) butane in NaCl solutions as a function of the temperature and NaCl molality.

butane+methane hydrates' initial configurations are in a 2 × 2 × 2 supercell, with a 17.31 Å lattice parameter for an sII unit cell.[81] For this binary hydrate, methane molecules are occupied in the sixteen 5^{12} cages, and butane molecules are put in the eight $5^{12}6^4$ cages in the sII unit hydrate cell.

For all systems, the cutoff radius for both the LJ and the short-range part of the Coulombic interactions is set at 12 Å. The particle−particle particle-mesh (PPPM)[83] method is used to calculate the long-range electrostatic interactions, with a relative error of 10^{-5}. The initial configurations, for both sI and sII structures, are first subjected to minimization using the Polak-Ribiere version of the conjugate gradient (CG) algorithm.[84] An equilibration simulation of 2 ns is followed by an isothermal−isobaric (constant-temperature, constant-pressure) ensemble

https://doi.org/10.1021/acs.jced.3c00225
J. Chem. Eng. Data 2024, 69, 3330−3346

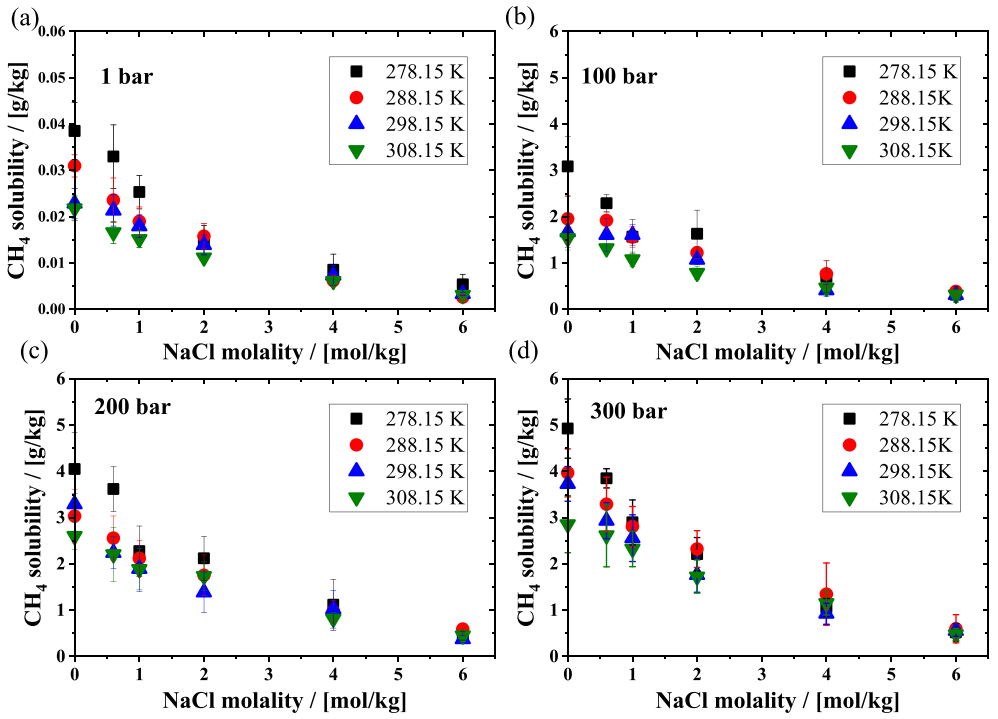

Figure 4. Solubilities of methane in NaCl solutions as a function of NaCl molality in solution at different pressures (a) 1, (b) 100, (c) 200, and (d) 300 bar and temperatures in the range (278.15−308.15) K.

simulation. The Nose-Hoover thermostat and barostat are used for temperature and pressure coupling with thermostat and barostat constants of 0.1 and 1.0 ps, respectively.[85] The Verlet algorithm[86] was utilized to integrate Newton's equations of motion with a time step of 1 fs. The periodic boundary conditions were applied in all directions of the systems.

Transport properties were calculated by on-the-fly computation using the transport property plugin (OCTP) in LAMMPS.[87] The plugin calculates the transport coefficients based on the mean-squared displacements (MSDs) of the dynamical properties obtained from the MD simulation. Specifically, the transport coefficients are determined as the slopes of the MSDs, which are plotted as linear functions of time. The self-diffusivity D_{Self}^{MD} and viscosity η can be directly computed in MD simulations using Einstein relations[88]

$$D_{Self}^{MD} = \lim_{t\to\infty} \frac{1}{6N_i t} \left\langle \sum_{j=1}^{N_i} (r_{j,i}(t) - r_{j,i}(0))^2 \right\rangle \tag{7}$$

and

$$\eta = \lim_{t\to\infty} \frac{1}{2t} \frac{V}{k_B T} \left\langle \left(\int_0^t P_{\alpha\beta}(t')\, dt \right)^2 \right\rangle \tag{8}$$

where N_i is the number of the specific molecule i in the system, and $r_{j,i}(t)$ and $r_{j,i}(0)$ are the positions of the j-th molecule of species i at time t and 0, respectively. $P_{\alpha\beta}(t')$ denotes the off-diagonal elements of the stress tensor at time t; V is the system volume, and the brackets $\langle ... \rangle$ are the ensemble averages.

To remove the effect of the system size in MD simulations, Yeh and Hummer[48] deduced a finite-size correction term using hydrodynamics, defined as the Yeh-Hummer (YH) correction

$$D_{Self}^{\infty} = D_{Self}^{MD} + \frac{k_B T \xi}{6\pi\eta L} \tag{9}$$

where D_{Self}^{MD} represents the finite self-diffusion coefficient obtained from MD simulations, k_B is the Boltzmann constant, T is the absolute temperature, η is the shear viscosity obtained from the simulation (the value of η is independent of the system size),[48,89−91] and ξ is a constant with a value of 2.837298 for periodic lattices, as discussed by previous studies.[49,92]

For transport property calculations, the simulation temperature range is 278.15−308.15 K, and the pressure is 1 bar. For the simulations of expansion coefficients for the four corresponding hydrates, the temperature range is 150−300 K at 145 bar. For the calculation of gas hydrate compressibility, the temperature is fixed at 287.15 K, and the pressure range is 50−7000 bar.

3. RESULTS AND DISCUSSION

3.1. Correction Factor k_{ij} for Alkane Groups and Water.

In Docherty's work,[34] the correction factor (k_{ij} = 1.07) for methane and water was optimized from the simulation of the excess chemical potential of methane in water using Widom's test particle method. Using this factor, we utilized a CFCMC simulation to compute the excess chemical potentials of methane in water at 1 bar across a range of temperatures. The results are shown in Figure S1 of the Supporting Information. Compared to Docherty's simulation[34] and Paschek's experimental[93] results, the numerical results of excess chemical potentials of methane in water are accurate with a small error at 298.15 K and 1 bar. Therefore, we chose this value of k_{ij} to describe the methane-water interaction and calculate the excess chemical potentials, solubilities, and self-diffusion coefficients of methane in NaCl solutions at different molalities, temperatures, and pressures.

The simulation results for the excess chemical potential of ethane in water using different force field combinations for ethane and water molecules at 298.15 K and 1 bar are shown in Table S5 of the Supporting Information. The reference value of

https://doi.org/10.1021/acs.jced.3c00225
J. Chem. Eng. Data 2024, 69, 3330−3346

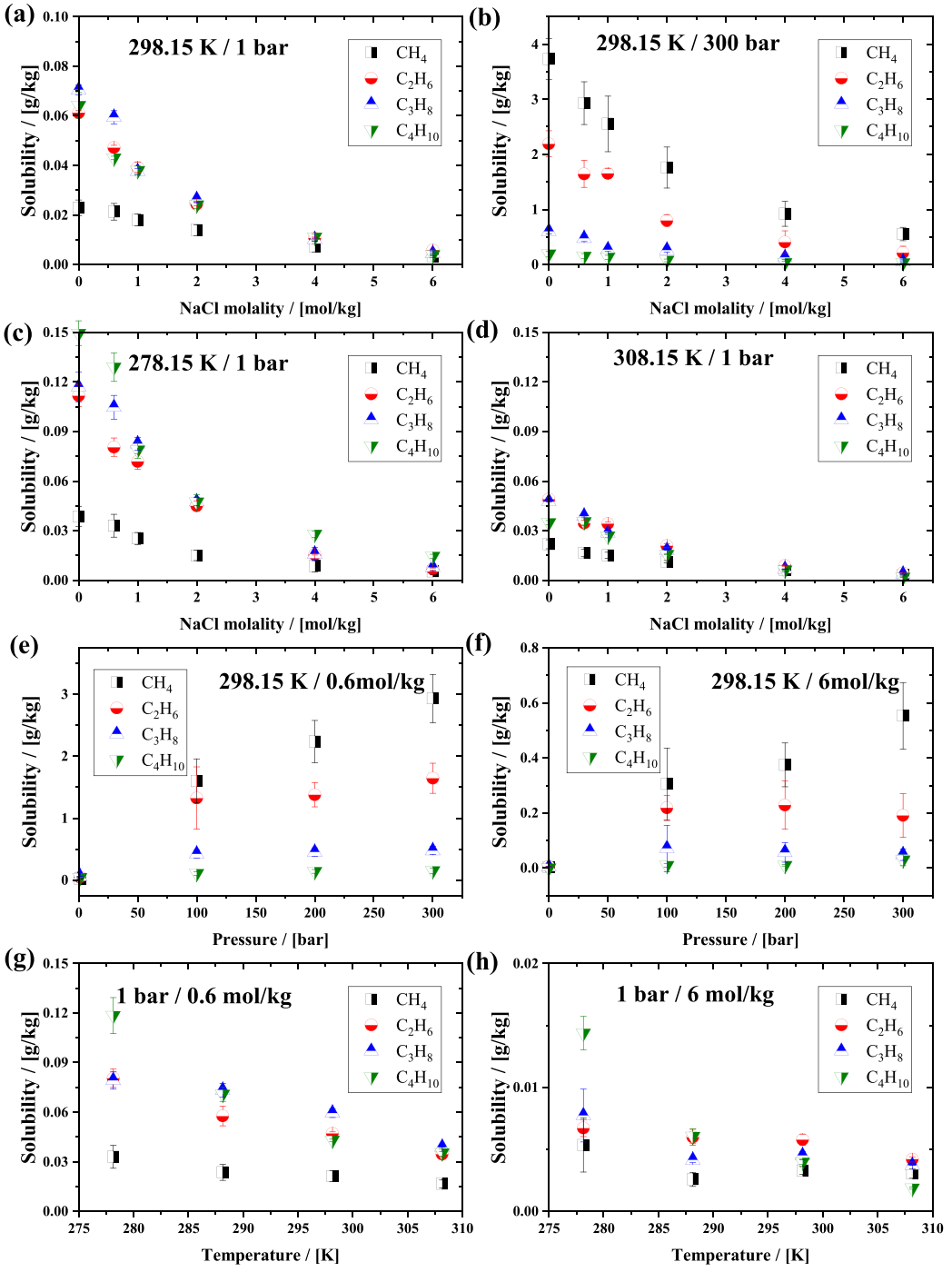

Figure 5. Solubilities of the four light *n*-alkanes as a function of NaCl molality at (a) 298.15 K and 1 bar, (b) 298.15 K and 300 bar, (c) 278.15 K and 1 bar, (d) 308.15 K and 1 bar; Solubilities of the four light *n*-alkanes as a function of pressure at (e) 298.15 K and 0.6 mol/kg NaCl molality, (f) 298.15 K and 6 mol/kg NaCl molality; Solubilities of the four light *n*-alkanes as a function of temperature at (g) 1 bar and 0.6 mol/kg NaCl molality, (h) 1 bar and 6 mol/kg NaCl molality.

the excess chemical potential was calculated using the experimental ethane solubility[29] which is equal to 7.59 kJ/mol. As shown in Figure 2c, the difference between the simulation value and the reference results (calculated using the solubility experimental value) appears systematically (all the calculated values of the excess chemical potential are larger than the reference values at different temperatures) with temperature. This phenomenon is similar to the calculation of the methane excess chemical potential in water.[34] Therefore, we increased the well depth of the CH_3 group−water LJ interaction to correct the interactions between ethane and water, which is the same as in the study by Docherty.[34] As shown in Figure 2a, by increasing the value of k_{ij}, the value of the excess chemical potential of ethane ($\mu^{ex}_{C_2H_6}$) in water at 298.15 K and 1 bar decreases. The computed value of $\mu^{ex}_{C_2H_6}$ is the closest to the experimental fitting value when $k_{ij} = 1.04$. The difference between the simulation and reference value (calculated using the solubility experimental value) is only 0.12 kJ/mol (relative error 1.58%). Using this k_{ij}, the excess chemical potentials of ethane in water at 1 bar and

https://doi.org/10.1021/acs.jced.3c00225
J. Chem. Eng. Data 2024, 69, 3330−3346

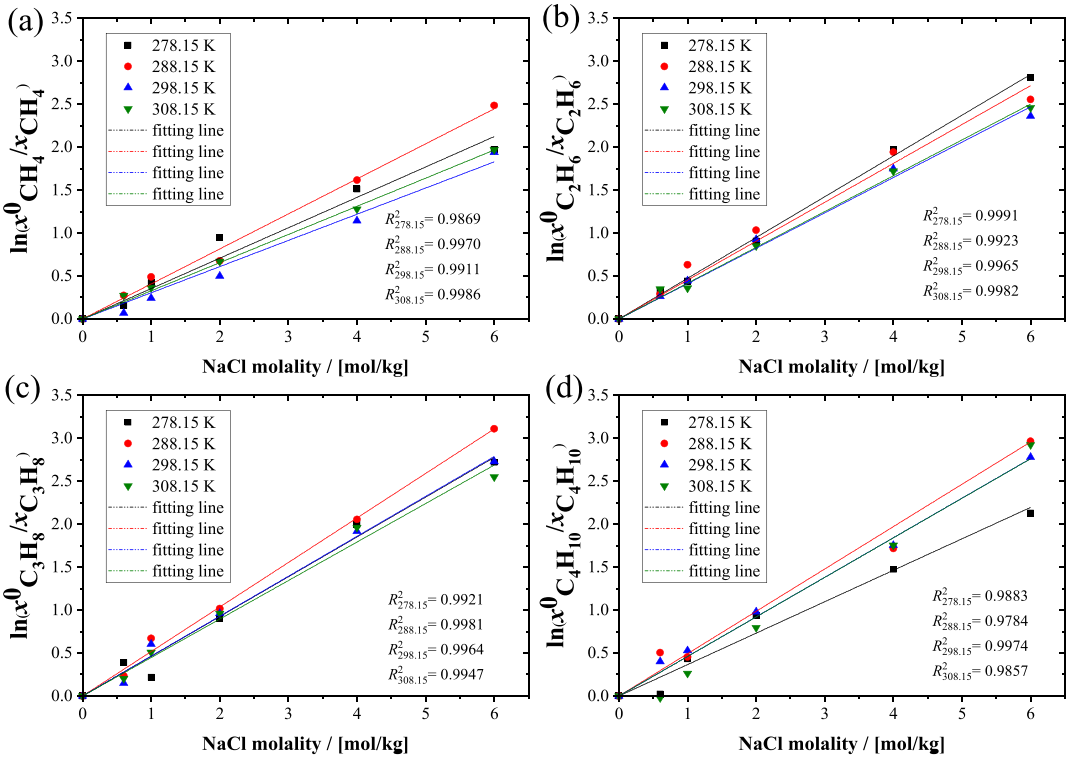

Figure 6. Ratio of logarithms of molar fractions of methane computed by MC simulations for the four alkanes as a function of NaCl molality in water as well as the fitting lines.

Table 2. Setschenow Coefficients k_{salt} of Alkanes as a Function of Temperature at 1 bar

	Methane	Ethane	Propane	Butane
278.15 K	0.35 ± 0.018	0.47 ± 0.006	0.463 ± 0.018	0.37 ± 0.017
288.15 K	0.40 ± 0.010	0.45 ± 0.017	0.51 ± 0.01	0.493 ± 0.03
298.15 K	0.305 ± 0.013	0.412 ± 0.01	0.465 ± 0.012	0.461 ± 0.01
308.15	0.327 ± 0.005	0.416 ± 0.007	0.448 ± 0.014	0.46 ± 0.02
ref value[94]	0.319	0.399	0.461	0.521

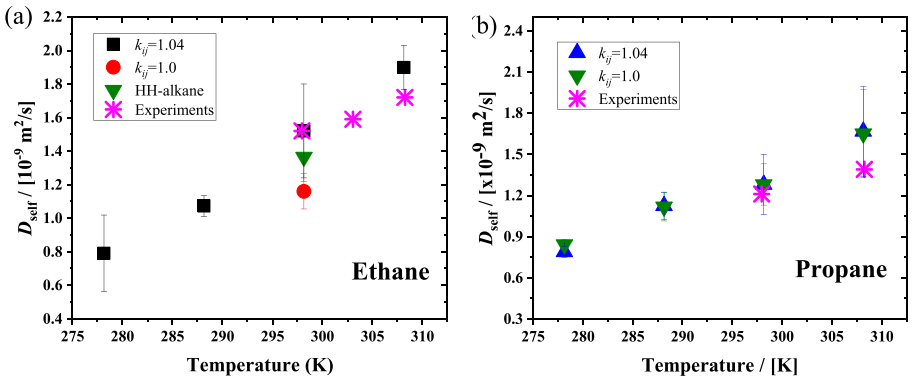

Figure 7. Self-diffusion coefficients of (a) ethane and (b) propane in water as a function of the temperature at 1 bar. The diffusivities are corrected by the finite-size effects.

different temperatures are computed. The simulation results are listed in Figure 2c. Clearly, the combination of the TIP4P/2005 model for water, the TraPPE model for ethane, and the modification of the interaction energy of the CH_3 group and water oxygen in the Lorentz-Bethelot combining rules yields good agreement with the reference values of the excess chemical potential for the whole temperature range.

The excess chemical potentials of propane in water at different temperatures are shown in Figure 2d. Without optimizing the interaction between propane and water, the simulation results for $\mu^{ex}_{C_3H_8}$ are larger than those of the experimental value. This indicates that the polarization of propane in water should not be ignored in excess chemical potential calculations. In the propane-water system, both CH_3 group-water and CH_2 group-water LJ interactions should be considered. Here, k_{ij} for the

https://doi.org/10.1021/acs.jced.3c00225
J. Chem. Eng. Data 2024, 69, 3330−3346

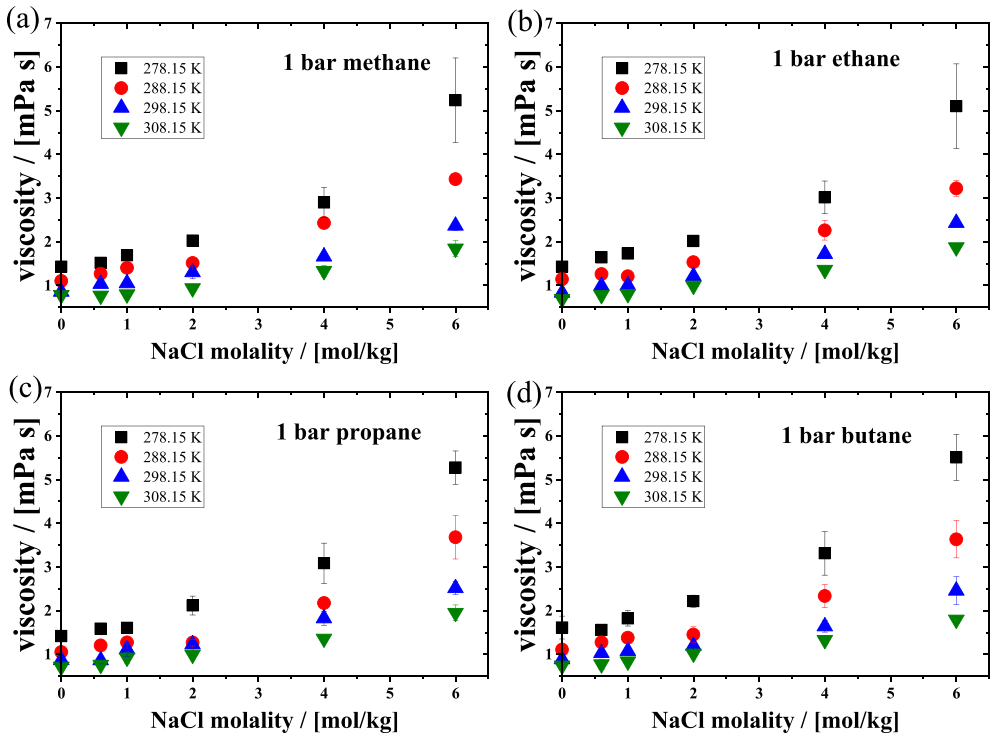

Figure 8. Simulated viscosities of NaCl solutions with (a) methane, (b) ethane, (c) propane, and (d) butane at different temperatures as a function of NaCl molality.

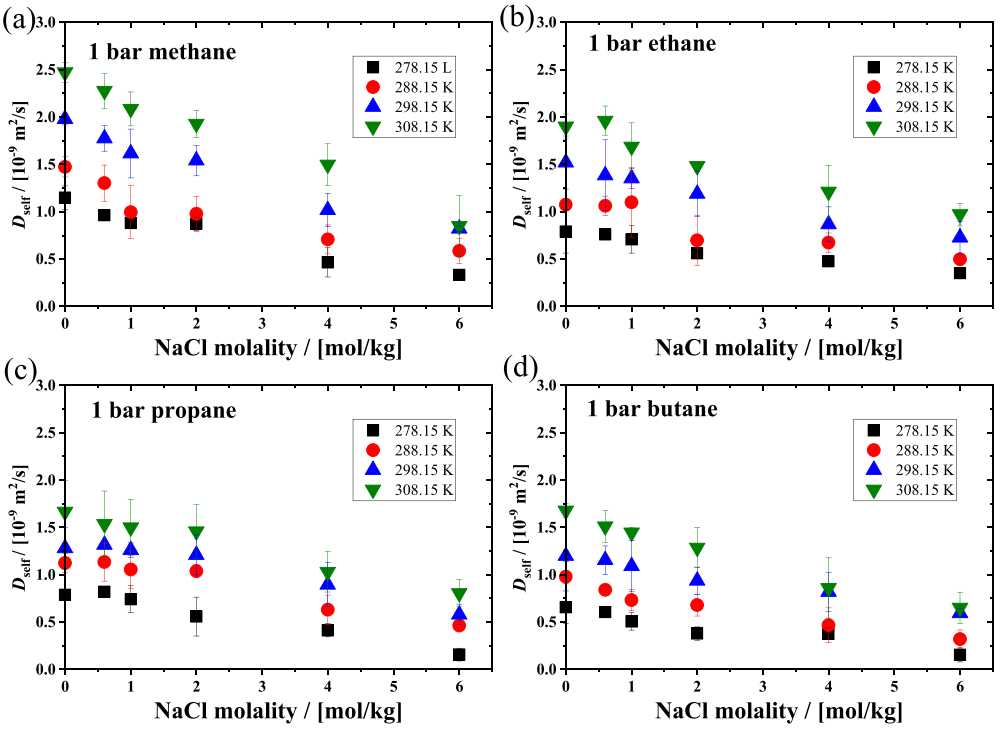

Figure 9. Computed self-diffusion coefficients of (a) methane, (b) ethane, (c) propane, and (d) butane in NaCl aqueous solutions as a function of NaCl molality at different temperatures and 1 bar.

interaction between CH_3 and water is fixed at 1.04; similarly, we vary the value of k_{ij} between CH_2 and water, and the results are shown in Figure 2b. The performance is the best when k_{ij} for the interaction between the CH_2 group and water is equal to 1. This indicates that the interaction between propane and water is mainly determined by the two CH_3 groups. Using the two k_{ij} values, the simulated values at different temperatures and 1 bar are in agreement with the experimental results. Therefore, to compute the excess chemical potentials and solubilities of the light *n*-alkanes in NaCl solutions, we used the correction factor k_{ij} = 1.04 to correct the interaction between the CH_3 group and

https://doi.org/10.1021/acs.jced.3c00225
J. Chem. Eng. Data 2024, 69, 3330−3346

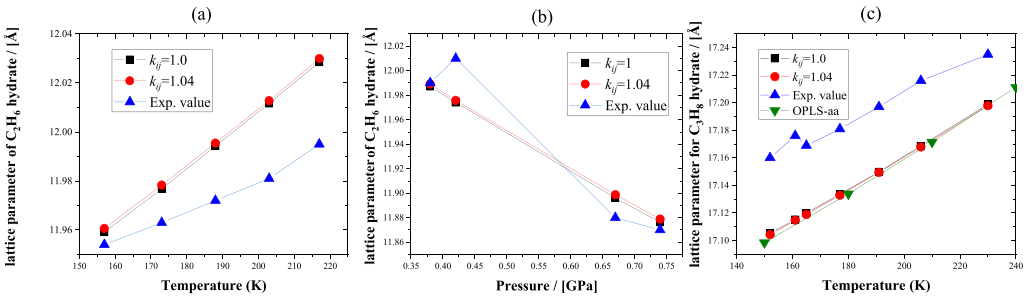

Figure 10. Lattice parameters of (a,b) ethane and (c) propane hydrates at various temperatures and pressures by using MD simulations, along with the experimental measurement results.

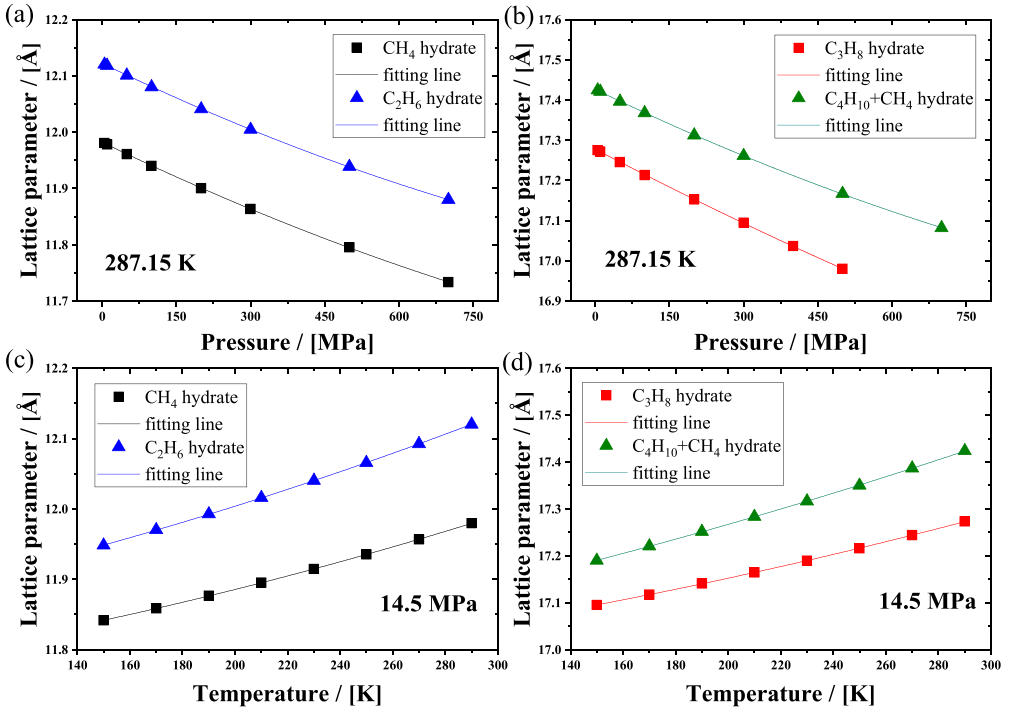

Figure 11. Lattice parameters of the sI and sII structure hydrates with the four *n*-alkanes as a guest molecule as a function of temperature and pressure. Methane and ethane hydrates are in structure I and shown in parts (a) and (c); propane and *n*-butane+methane hydrates are in structure II, and the simulation results are shown in parts (b) and (d).

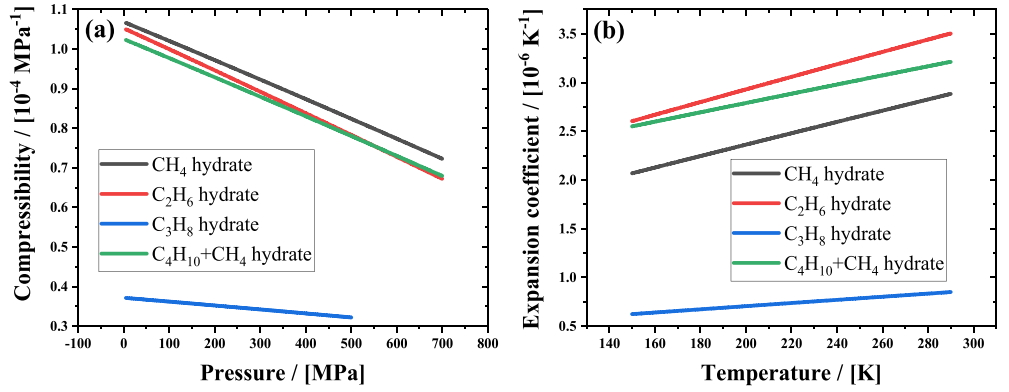

Figure 12. Isothermal compressibilities (a) and thermal expansion coefficients (b) of the hydrate crystals with the four *n*-alkanes in H-bonded cages.

water and k_{ij} = 1 for the interaction between the CH_2 group and water at different temperatures and pressures.

3.2. Excess Chemical Potentials and Solubilities of the Four Alkanes in NaCl Aqueous Solutions. In Figure 3, the computed excess chemical potentials of the four *n*-alkanes in the NaCl solution as a function of NaCl molality at 1 bar and different temperatures are shown. For a fixed molality, the higher the temperature, the larger the excess chemical potential of alkanes in NaCl solutions. By increasing the NaCl molality, the excess chemical potential of alkanes in the NaCl solution

https://doi.org/10.1021/acs.jced.3c00225
J. Chem. Eng. Data 2024, 69, 3330−3346

increases linearly. At identical conditions of temperature and molality, the excess chemical potentials of the four alkanes exhibit variations, especially at high concentrations of NaCl in water.

Based on the excess chemical potentials shown in Figure 3, we can obtain the Henry coefficients using Eq 5 and the solubilities of the four alkanes in the NaCl solution by Eq 6 at 1 bar. The solubilities of methane in the NaCl solution at 1 bar are shown in Figure 4a. Methane solubilities in the NaCl solution as a function of temperature and NaCl molality at 100, 200, and 300 bar are shown in Figures 4b, 4c, and 4d, respectively. As expected, the solubility of methane decreased with decreasing pressure and increasing temperature. As shown in Figures 4a and 4b, the solubility of methane increases significantly (ca. 2 orders of magnitude) from 1 to 100 bar under the same temperature conditions. At even higher pressures (Figures 4b, 4c, and 4c), increasing the pressure from 100 to 300 bar leads to slightly higher alkane solubilities. Besides the temperature and pressure trends, the experimentally observed salting out phenomena are captured by the simulations.[30] When the molality of NaCl in water increases, the solubility of methane decreases. At low NaCl molalities (below 2 mol/kg), increasing the temperature from 278.15 to 308.15 K leads to lower methane solubilities at the same pressures, so the temperature effect cannot be ignored. As the molality of a solution increases, the solubility becomes less affected by changes in the temperature and more influenced by the concentration of the salts. The effect of pressure on methane solubility in water also weakens with increasing NaCl molalities.

The solubilities of ethane, propane, and butane *n*-alkanes as a function of NaCl molality at different temperatures and pressures are shown in Figures S2−S4 of the Supporting Information. Figure 5 shows the solubilities of the four alkanes at various temperatures, pressures, and NaCl molality in the solution. As shown in Figures 5a-5d, the solubilities of alkanes decrease as the molality of NaCl in water increases. Additionally, Figures 5e and 5f show that decreasing pressure also decreases solubility, while Figures 5g and 5h show that solubility decreases as the temperature increases. The simulation results clearly indicate the salting out effect for all alkanes in the NaCl solutions. At a temperature of 298.15 K and a pressure of 1 bar (Figure 5a), methane exhibits the lowest solubility among the four alkanes, and the solubilities of the other three alkanes are comparable to each other at the same molalities. At 300 bar (Figure 5b), the differences among the solubilities of the four types of alkanes are very pronounced; the solubilities decrease with the carbon number. When the pressure is increased from 1 to 300 bar, the solubility of alkanes increases significantly (1−2 orders of magnitude). As can be seen in Figures 5c and 5d, the solubilities of the four alkanes in the NaCl solution decrease as the temperature increases. At higher NaCl molalities, the difference in the solubility of the four alkane molecules in water becomes less pronounced. At ca. 6 mol/kg, which is close to the saturation solubility of NaCl in water, the solubilities of the four alkanes become almost the same. At 298.15 K, the solubility of the four alkanes increases significantly if the pressure increases from 1 to 100 bar (Figures 5e and 5f). The solubility of methane in the NaCl solution increases further in the pressure range of 100−300 bar, whereas for the other three alkanes, the solubilities vary only weakly. This indicates that the solubility of *n*-alkanes in the NaCl solution is sensitive to pressure within a specific range, which depends on the alkane. This result holds for both the low and the high NaCl molalities. As shown in Figures 5g and 5h, at 1 bar and low NaCl molalities (0.6 mol/kg), the differences between the solubilities of the four types of alkanes are pronounced at the same temperatures; at high NaCl molalities (6 mol/kg), the differences in solubilities decrease, and the solubilities become mainly dependent on the NaCl molality for all four types of alkanes.

By calculation of the solubilities of alkanes in the NaCl solution at different molalities, the empirical Setschenow equation (Eq 1) can be used to describe the salting out effect. The ratios of logarithms of the mole fractions of the alkanes as a function of NaCl molalities computed in the CFCMC simulations are shown in Figure 6. We used a linear function to establish the relationship between the ratio and molality, and the fitting lines, which have a high determination coefficient, are shown in Figure 6. In Table 2, the Setschenow coefficients of the four alkanes are listed at different temperatures and 1 bar. The simulation results are in good agreement with the reference results.[94] As expected, the salting out coefficient is almost temperature independent for the four light alkanes.

3.3. Self-Diffusion Coefficients of the Four Alkanes in NaCl Aqueous Solutions. In Section 3.1, we showed the energy interaction between the CH_3/CH_2 group and water by CFCMC calculation of the excess chemical potential at 298.15 K and 1 bar. The correction factor k_{ij} for CH_3 and water is 1.04, and the correction factor k_{ij} for CH_2 and water is 1. Here, MD simulations were performed to calculate the self-diffusion coefficients of alkanes in pure water at different temperatures using eq 9. The results for ethane and propane with and without using the correction factor k_{ij} are shown in Figure 7, along with the experimental results.[43−45] For ethane (Figure 7a), the computed self-diffusion coefficients using the optimized value k_{ij} = 1.04 in the Lorentz-Bethelot combining rules are in agreement with the experiments at 298.15 K and 1 bar. The performance of the force field combination (TIP4P/2005 for water and TraPPE for ethane) with a correction factor is better than that of the HH-alkane force field and TraPPE without modification (k_{ij} = 1 for CH_3 and water). At 308.15 K, the difference in the self-diffusion coefficient between the simulation and experimental results becomes pronounced, which may be attributed to the correction factor being optimized at 298.15 K and 1 bar, at different temperatures; this value of k_{ij} may not describe the interaction between ethane and water well. The self-diffusion coefficients for propane are listed in Figure 7(b). Practically, there is no obvious difference in the self-diffusion coefficients when using the correction factor k_{ij}. These results indicate that the correction factor fitting by the excess chemical potential also performs well in the calculation of diffusion coefficients.

Using the correction factor k_{ij} obtained in this work, the calculated viscosities for the four systems as a function of NaCl molality in water at 1 bar and various temperatures are shown in Figure 8. The shear viscosity of the system increases with increasing NaCl molality and temperature. The contribution of alkanes to the shear viscosity of the system is relatively small because alkanes are nonpolar molecules that do not engage in hydrogen bonding or ionic interactions with water molecules or ions. Since viscosity is the result of intermolecular interactions in solution, and there is only a single alkane molecule in each MD simulation, the effect of alkane-alkane on the viscosity of a NaCl aqueous solution is absent.

The self-diffusion coefficients of the four alkanes in the NaCl aqueous solution as a function of NaCl molalities at different temperatures are shown in Figure 9. With an increase in temperature, the self-diffusion coefficients of the alkanes

https://doi.org/10.1021/acs.jced.3c00225
J. Chem. Eng. Data 2024, 69, 3330−3346

Table 3. Calculated Solubilities of the Four Light Alkanes in NaCl Solutions as a Function of NaCl Molality, Temperature, and Pressure[a]

			Methane		Ethane		Propane		Butane	
T	P	M	S	$u(s)$	S	$u(s)$	S	$u(s)$	S	$u(s)$
278.15	1	0	0.038	0.006	0.111	0.006	0.117	0.008	0.149	0.007
278.15	1	0.6	0.032	0.006	0.080	0.005	0.079	0.005	0.129	0.008
278.15	1	1	0.025	0.003	0.072	0.004	0.094	0.002	0.078	0.005
278.15	1	2	0.014	0.003	0.045	0.003	0.047	0.002	0.047	0.004
278.15	1	4	0.008	0.003	0.0155	0.0002	0.015	0.004	0.027	0.001
278.15	1	6	0.005	0.002	0.0067	0.0007	0.007	0.002	0.014	0.001
288.15	1	0	0.031	0.002	0.077	0.007	0.092	0.004	0.11	0.01
288.15	1	0.6	0.023	0.004	0.057	0.005	0.073	0.004	0.071	0.004
288.15	1	1	0.019	0.003	0.041	0.002	0.047	0.001	0.074	0.003
288.15	1	2	0.016	0.002	0.027	0.002	0.033	0.001	0.028	0.001
288.15	1	4	0.006	0.001	0.0110	0.0009	0.0118	0.005	0.021	0.002
288.15	1	6	0.0025	0.0005	0.0059	0.0006	0.0041	0.0002	0.0060	0.0005
298.15	1	0	0.023	0.003	0.0613	0.0008	0.070	0.002	0.064	0.005
298.15	1	0.6	0.021	0.003	0.0471	0.0009	0.059	0.002	0.0430	0.0006
298.15	1	1	0.018	0.002	0.039_1	0.001	0.037	0.001	0.037	0.001
298.15	1	2	0.014	0.002	0.0243	0.0005	0.026	0.001	0.024	0.001
298.15	1	4	0.007	0.002	0.0106	0.0003	0.0101	0.0005	0.011	0.001
298.15	1	6	0.0033	0.0003	0.0057	0.0004	0.0045	0.0003	0.0039	0.0002
308.15	1	0	0.022	0.002	0.0489	0.0009	0.0475	0.0001	0.034	0.001
308.15	1	0.6	0.016	0.002	0.034	0.001	0.03882	0.00006	0.035	0.002
308.15	1	1	0.015	0.001	0.0341	0.0009	0.02857	0.00003	0.0267	0.0009
308.15	1	2	0.0111	0.0007	0.0209	0.0009	0.01818	0.00004	0.0156	0.0003
308.15	1	4	0.0061	0.0008	0.0087	0.0003	0.00669	0.00008	0.0060	0.0007
308.15	1	6	0.0030	0.0003	0.0042	0.0002	0.00371	0.00001	0.0018	0.0008
278.15	100	0	3.1	0.6	2.4	0.3	0.6	0.1	0.25	0.06
278.15	100	0.6	2.3	0.1	2.1	0.6	0.45	0.08	0.16	0.09
278.15	100	1	1.5	0.3	1.5	0.5	0.4	0.1	0.15	0.05
278.15	100	2	1.6	0.5	1.0	0.4	0.20	0.04	0.13	0.08
278.15	100	4	0.7	0.3	0.5	0.2	0.08	0.06	0.003	0.003
278.15	100	6	0.3	0.1	0.2	0.1	0.02	0.01	0.01	0.01
288.15	100	0	1.9	0.5	2.3	0.1	0.6	0.1	0.24	0.06
288.15	100	0.6	1.9	0.1	1.7	0.3	0.4	0.1	0.13	0.09
288.15	100	1	1.5	0.2	1.1	0.3	0.3	0.1	0.11	0.03
288.15	100	2	1.2	0.1	0.8	0.2	0.29	0.08	0.07	0.08
288.15	100	4	0.7	0.2	0.34	0.7	0.12	0.07	0.04	0.03
288.15	100	6	0.38	0.06	0.22	0.09	0.04	0.02	0.04	0.03
298.15	100	0	1.7	0.3	1.6	0.3	0.5	0.1	0.2	0.1
298.15	100	0.6	1.6	0.3	1.3	0.5	0.42	0.06	0.10	0.2
298.15	100	1	1.6	0.2	1.2	0.3	0.26	0.06	0.10	0.5
298.15	100	2	1.1	0.1	0.6	0.1	0.22	0.01	0.033	0.009
298.15	100	4	0.40	0.01	0.3	0.1	0.09	0.04	0.014	0.006
298.15	100	6	0.3	0.1	0.22	0.04	0.07	0.08	0.009	0.006
308.15	100	0	1.5	0.2	1.6	0.2	0.45	0.07	0.14	0.03
308.15	100	0.6	1.31	0.09	1.1	0.3	0.36	0.04	0.09	0.02
308.15	100	1	1.1	0.1	1.3	0.3	0.27	0.06	0.07	0.01
308.15	100	2	0.8	0.1	0.9	0.3	0.16	0.04	0.05	0.01
308.15	100	4	0.5	0.1	0.36	0.05	0.09	0.01	0.022	0.005
308.15	100	6	0.3	0.1	0.25	0.07	0.04	0.01	0.008	0.006
278.15	200	0	4.0	0.7	2.6	0.5	0.9	0.2	0.20	0.07
278.15	200	0.6	3.6	0.4	1.6	0.3	0.5	0.1	0.17	0.009
278.15	200	1	2.3	0.5	1.4	0.4	0.5	0.1	0.16	0.03
278.15	200	2	2.1	0.4	1.0	0.2	0.3	0.1	0.08	0.02
278.15	200	4	1.1	0.5	0.6	0.1	0.09	0.02	0.04	0.02
278.15	200	6	0.44	0.09	0.2	0.1	0.06	0.06	0.015	0.007
288.15	200	0	3.0	0.5	2.5	0.4	0.7	0.1	0.18	0.06
288.15	200	0.6	2.5	0.4	1.5	0.2	0.4	0.1	0.1	0.1
288.15	200	1	2.1	0.3	1.3	0.2	0.3	0.1	0.06	0.03
288.15	200	2	1.7	0.4	0.9	0.2	0.23	0.08	0.05	0.01

https://doi.org/10.1021/acs.jced.3c00225
J. Chem. Eng. Data 2024, 69, 3330−3346

Table 3. continued

			Methane		Ethane		Propane		Butane	
T	P	M	S	$u(s)$	S	$u(s)$	S	$u(s)$	S	$u(s)$
288.15	200	4	0.9	0.2	0.4	0.1	0.09	0.05	0.02	0.01
288.15	200	6	0.6	0.1	0.14	0.07	0.02	0.01	0.02	0.01
298.15	200	0	3.3	0.2	1.8	0.1	0.7	0.1	0.17	0.06
298.15	200	0.6	2.2	0.3	1.3	0.1	0.45	0.06	0.14	0.02
298.15	200	1	1.9	0.4	1.3	0.4	0.25	0.06	0.10	0.05
298.15	200	2	1.4	0.4	0.7	0.2	0.27	0.07	0.05	0.03
298.15	200	4	1.0	0.4	0.40	0.03	0.11	0.02	0.023	0.008
298.15	200	6	0.37	0.07	0.22	0.08	0.05	0.03	0.009	0.002
308.15	200	0	2.6	0.3	1.9	0.1	0.7	0.1	0.14	0.03
308.15	200	0.6	2.2	0.5	1.5	0.1	0.48	0.09	0.11	0.02
308.15	200	1	1.9	0.4	1.0	0.2	0.4	0.2	0.10	0.01
308.15	200	2	1.7	0.3	0.8	0.2	0.19	0.09	0.07	0.02
308.15	200	4	0.8	0.1	0.37	0.09	0.11	0.04	0.02	0.01
308.15	200	6	0.4	0.1	0.17	0.08	0.04	0.02	0.014	0.007
278.15	300	0	4.9	0.6	2.8	0.5	0.8	0.1	0.35	0.04
278.15	300	0.6	3.8	0.2	1.8	0.5	0.7	0.1	0.20	0.07
278.15	300	1	2.9	0.4	1.7	0.2	0.64	0.09	0.15	0.04
278.15	300	2	2.2	0.3	1.3	0.2	0.3	0.1	0.10	0.03
278.15	300	4	1.1	0.1	0.7	0.1	0.12	0.06	0.08	0.05
278.15	300	6	0.5	0.1	0.20	0.07	0.07	0.04	0.01	0.01
288.15	300	0	3.9	0.5	2.7	0.6	0.9	0.2	0.25	0.03
288.15	300	0.6	3.3	0.5	2.1	0.1	0.6	0.1	0.18	0.03
288.15	300	1	2.8	0.4	1.6	0.6	0.3	0.1	0.13	0.05
288.15	300	2	2.3	0.3	1.3	0.7	0.41	0.06	0.10	0.06
288.15	300	4	1.3	0.6	0.8	0.5	0.11	0.07	0.02	0.01
288.15	300	6	0.6	0.5	0.2	0.1	0.06	0.02	0.01	0.01
298.15	300	0	3.7	0.3	2.2	0.2	0.60	0.05	0.19	0.05
298.15	300	0.6	2.9	0.3	1.6	0.2	0.47	0.06	0.15	0.04
298.15	300	1	2.5	0.5	1.65	0.08	0.26	0.02	0.13	0.04
298.15	300	2	1.7	0.3	0.8	0.1	0.25	0.03	0.07	0.02
298.15	300	4	0.9	0.2	0.4	0.2	0.12	0.03	0.03	0.02
298.15	300	6	0.5	0.1	0.19	0.07	0.04	0.02	0.02	0.02
308.15	300	0	2.8	0.6	1.9	0.3	0.66	0.06	0.16	0.04
308.15	300	0.6	2.6	0.6	1.5	0.2	0.47	0.05	0.097	0.008
308.15	300	1	2.3	0.3	1.3	0.3	0.3	0.1	0.104	0.007
308.15	300	2	1.7	0.3	0.9	0.2	0.20	0.07	0.06	0.02
308.15	300	4	1.1	0.2	0.5	0.2	0.14	0.06	0.02	0.01
308.15	300	6	0.4	0.1	0.3	0.1	0.04	0.01	0.013	0.005

[a] T is temperature in units of K; P is the pressure in units of bar; M is the molality of NaCl in units of mol/kg; S is solubility; $u(s)$ is the standard uncertainty, and the units of S and $u(s)$ are g/kg. These uncertainties are calculated based on the results of five independent simulations for each condition (concentration, temperature, and pressure).

increase, and the self-diffusion coefficients decrease with increasing NaCl molality. At the same temperature and NaCl molality, the self-coefficient decreases with an increase in the number of carbons in the *n*-alkane.

3.4. Thermodynamics Properties of the Alkanes' Corresponding Hydrate Crystals. Gas hydrates are composed of *n*-alkanes and water in the solid phase. We calculated the lattice parameter of ethane and propane hydrates at different temperature and pressure conditions as shown in Figure 10. The results are compared with the experimental measurements of Hester[52] and Manakov.[53] The simulation results are consistent with the experimental results for a wide temperature and pressure range. The simulation results obtained using k_{ij} = 1.0 (without correction) and k_{ij} = 1.04 for the CH_3 group and water interaction are almost identical. This indicates that the correction factor optimized in this study also describes the hydrate crystal system.

To investigate the effect of pressure and temperature on the lattice parameter, the temperature was first set to 287.15 K, and the pressure was varied from 5 to 700 MPa. The lattice parameters of the methane hydrate, ethane hydrate, propane hydrate, and butane+methane binary hydrate are shown in Figures 11(a) and 11(b). The lattice parameters of the hydrate decrease with an increasing pressure. The H-bonded network framework formed by host water molecules in hydrate crystals can be compressed, while the guest−host interactions ensure the stability of the crystal at high pressure. Subsequently, the pressure was set to 14.5 MPa, and the temperature was varied from 150 to 290 K. Lattice parameters of those hydrates are shown in Figures 11(c) and 11(d). The lattice parameters of the hydrate increase with an increasing temperature. Both methane and ethane hydrates form structure I. The lattice parameter of ethane hydrate is larger than that of methane hydrate at the same temperature and pressure. Propane hydrate and butane

https://doi.org/10.1021/acs.jced.3c00225
J. Chem. Eng. Data 2024, 69, 3330−3346

Table 4. Calculated Viscosities of Aqueous NaCl Solutions with One Alkane Molecule in Systems and Self-Diffusion Coefficients for the Four Alkanes in NaCl Solutions as a Function of Temperature and Pressure[a]

			Methane		Ethane		Propane		Butane	
T	P	M	η	$u(\eta)$	η	$u(\eta)$	η	$u(\eta)$	η	$u(\eta)$
278.15	1	0	1.42	0.04	1.42	0.05	1.41	0.07	1.6	0.2
278.15	1	0.6	1.51	0.04	1.64	0.08	1.58	0.08	1.5	0.1
278.15	1	1	1.68	0.04	1.73	0.05	1.60	0.03	1.8	0.1
278.15	1	2	2.02	0.05	2.0	0.1	2.1	0.2	2.2	0.1
278.15	1	4	2.8	0.3	3.0	0.3	3.0	0.4	3.3	0.4
278.15	1	6	5.2	0.9	5.1	0.9	5.2	0.3	5.5	0.5
288.15	1	0	1.10	0.07	1.1	0.1	1.05	0.03	1.10	0.06
288.15	1	0.6	1.27	0.09	1.2	0.1	1.20	0.01	1.27	0.09
288.15	1	1	1.4	0.1	1.21	0.03	1.27	0.03	1.38	0.09
288.15	1	2	1.51	0.03	1.53	0.03	1.26	0.07	1.4	0.1
288.15	1	4	2.43	0.04	2.2	0.1	2.17	0.06	2.3	0.2
288.15	1	6	3.43	0.03	3.2	0.1	3.6	0.4	3.6	0.4
298.15	1	0	0.85	0.02	0.83	0.03	0.86	0.05	0.88	0.04
298.15	1	0.6	1.03	0.02	0.98	0.06	0.86	0.08	1.03	0.06
298.15	1	1	1.05	0.05	1.00	0.06	1.1	0.1	1.07	0.08
298.15	1	2	1.3	0.1	1.21	0.03	1.22	0.07	1.19	0.01
298.15	1	4	1.66	0.05	1.72	0.05	1.8	0.1	1.6	0.1
298.15	1	6	2.3	0.1	2.43	0.06	2.5	0.1	2.4	0.3
308.15	1	0	0.783	0.002	0.69	0.03	0.72	0.05	0.74	0.09
308.15	1	0.6	0.7	0.1	0.78	0.05	0.76	0.02	0.7	0.1
308.15	1	1	0.79	0.01	0.80	0.05	0.9	0.1	0.83	0.02
308.15	1	2	0.93	0.04	0.99	0.07	0.99	0.07	1.02	0.06
308.15	1	4	1.33	0.05	1.35	0.02	1.36	0.04	1.32	0.05
308.15	1	6	1.8	0.1	1.87	0.04	1.9	0.1	1.79	0.08
			Methane		Ethane		Propane		Butane	
T	P	M	D_{Self}	$u(D_{Self})$	D_{Self}	$u(D_{Self})$	D_{Self}	$u(D_{Self})$	D_{Self}	$u(D_{Self})$
278.15	1	0	1.1	0.1	0.8	0.2	0.78	0.04	0.6	0.1
278.15	1	0.6	0.96	0.04	0.75	0.04	0.81	0.05	0.60	0.03
278.15	1	1	0.88	0.03	0.7	0.1	0.7	0.1	0.50	0.09
278.15	1	2	0.87	0.06	0.56	0.04	0.5	0.2	0.37	0.06
278.15	1	4	0.4	0.1	0.47	0.01	0.41	0.06	0.37	0.06
278.15	1	6	0.33	0.04	0.35	0.03	0.15	0.06	0.15	0.07
288.15	1	0	1.4	0.1	1.07	0.06	1.1	0.1	0.97	0.06
288.15	1	0.6	1.3	0.1	1.0	0.1	1.1	0.2	0.83	0.04
288.15	1	1	0.9	0.2	1.01	0.03	1.0	0.1	0.7	0.1
288.15	1	2	0.9	0.1	0.7	0.2	1.03	0.06	0.6	0.1
288.15	1	4	0.7	0.1	0.7	0.1	0.6	0.1	0.4	0.1
288.15	1	6	0.5	0.1	0.49	0.06	0.46	0.04	0.31	0.09
298.15	1	0	1.97	0.06	1.5	0.2	1.2	0.2	1.19	0.05
298.15	1	0.6	1.7	0.1	1.3	0.3	1.31	0.03	1.1	0.1
298.15	1	1	1.6	0.2	1.3	0.1	1.26	0.07	1.1	0.2
298.15	1	2	1.5	0.1	1.1	0.2	1.2	0.2	0.9	0.1
298.15	1	4	1.0	0.1	0.8	0.1	0.8	0.2	0.8	0.2
298.15	1	6	0.82	0.02	0.7	0.1	0.5	0.1	0.59	0.04
308.15	1	0	2.4	0.1	1.9	0.1	1.6	0.3	1.67	0.07
308.15	1	0.6	2.2	0.1	1.9	0.1	1.5	0.3	1.5	0.1
308.15	1	1	2.0	0.1	1.6	0.2	1.5	0.2	1.4	0.5
308.15	1	2	1.9	0.1	1.48	0.03	1.4	0.2	1.2	0.2
308.15	1	4	1.4	0.2	1.2	0.2	1.0	0.2	0.8	0.3
308.15	1	6	0.8	0.3	0.9	0.1	0.8	0.1	0.6	0.1

[a] T is temperature in units of K; P is the pressure in units of bar; M is the molality of NaCl in units of mol/kg; η is shear viscosity; $u(\eta)$ is the standard uncertainty; the units of η and $u(\eta)$ are mPa·s; D_{Self} is the self-diffusion coefficient; $u(D_{Self})$ is the standard uncertainty; and the units of D_{Self} and $u(D_{Self})$ are 10^{-9} m^2/s. These uncertainties are calculated based on the results of five independent simulations for each condition (concentration, temperature, and pressure).

+methane binary hydrate form structure II. The lattice parameter of butane+methane binary hydrate is larger than that of propane hydrate at the same temperature and pressure. The difference in the lattice parameter of hydrate is induced by the guest−host interactions. A guest molecule with a large van der Waals volume may cause the crystal to expand.[66,67,95]

https://doi.org/10.1021/acs.jced.3c00225
J. Chem. Eng. Data 2024, 69, 3330−3346

By calculating the lattice parameters (shown in Figure 11), the thermal expansion coefficient (α_P) and isothermal compressibility (κ_T) of hydrates can be calculated through numerical differentiation using the following equations

$$\alpha_P = \frac{1}{V}\left(\frac{\partial V}{\partial T}\right)_P \tag{10}$$

$$\kappa_T = -\frac{1}{V}\left(\frac{\partial V}{\partial P}\right)_T \tag{11}$$

where V is the volume of hydrate. The isothermal compressibilities and the thermal expansion coefficients of hydrates are shown in Figures 12 (a) and 12(b), respectively. The thermodynamic properties vary among hydrates formed with four different *n*-alkanes. For the four hydrates, propane hydrate has the lowest compressibility, because propane molecules only occupy the large cages in the sII hydrate crystal, leaving the small cage empty; there is no guest−host interaction in these small cages. The other three hydrates are all occupied, and the compressibilities of the hydrates are almost comparable to each other and much larger than that of propane hydrate (Figure 12a). For the expansion coefficient of hydrates as shown in Figure 12(b), ethane hydrate has the highest value of α_P, followed by butane+methane binary hydrate, methane hydrate, and propane hydrate. Apart from propane hydrate, the other hydrates have similar thermal expansivity and compressibility. These results are consistent with Hester's experiment results.[52] Among these hydrates, only propane hydrate has empty small cages, as it is not fully occupied by guest molecules. This leads to the hydrate crystal being resistant to compression and expansion. The two thermal properties become less dependent on the guest size and hydrate crystal type and are instead dominated by guest occupancy.

4. CONCLUSIONS

The solubilities and diffusion coefficients of four light *n*-alkanes (methane, ethane, propane, and *n*-butane) in aqueous NaCl solutions and the thermodynamics properties of their corresponding hydrate crystals are calculated by molecular simulations. To improve accuracy of the calculations, CFCMC simulations were performed to correct the interaction between alkane groups and water by fitting the calculated and experimental values of the excess chemical potential of ethane and propane in water at 1 bar and 298.15 K. The optimized correction factor k_{ij} for the interactions between CH_3 and water is 1.04, and k_{ij} between CH_2 and water is 1.0. Using these correction factors, the excess chemical potentials of four light *n*-alkanes (methane, ethane, propane, and *n*-butane) in aqueous NaCl solutions with different molalities (0−6 mol/kg) and temperatures (278.15 K−308.15 K) are calculated at 1 bar, and the solubilities of the four alkanes in aqueous NaCl solution are calculated using Henry's law. The solubilities of the four alkanes are calculated at high pressure (100, 200, and 300 bar) by using CFCMC simulations in the Gibbs Ensemble. All simulations are performed using the Brick-CFCMC software. Solubilities of the four alkanes depend on the temperature, pressure, and molality of NaCl in solution. Our simulation results show that the solubility of alkanes decreases with increasing salt molality, a phenomenon known as the salting out effect. The solubility data for each *n*-alkane at different conditions are listed in Table 3.

Using the correction factors k_{ij}, MD simulations are performed to calculate the transport properties of the four light *n*-alkanes in aqueous NaCl solutions at 1 bar and temperatures of 278.15 K−308.15 K. The shear viscosities of the aqueous solution systems with the alkanes and diffusion coefficients (D_{Self}) optimized by a finite-size correction of the four alkanes in solution with different NaCl molalities are obtained. The diffusion coefficients decrease as the carbon number increases in *n*-alkanes and as the system temperature decreases. The viscosity and diffusion coefficient data for each *n*-alkane at different conditions can be found in Table 4.

The lattice parameters of the four corresponding hydrates (methane hydrate, ethane hydrate, propane hydrate, and butane +methane binary hydrate) are computed for a wide range of temperatures (150−300) K and pressures (1−7000 bar) using MD simulations. The thermodynamic properties of the hydrates, including isothermal compressibility and the thermal expansion coefficient, are calculated by the numerical differentiation of the hydrate volume. The thermodynamic properties of the four hydrates differ from each other, particularly in the case of the propane hydrate due to the effects of host−guest interactions and guest occupancy.

■ ASSOCIATED CONTENT

Supporting Information

The Supporting Information is available free of charge at https://pubs.acs.org/doi/10.1021/acs.jced.3c00225.

Parameters for the force fields; Fugacity coefficients for the four light alkanes; excess chemical potentials of methane, ethane, and propane in water; solubilities of ethane, propane, and butane in the NaCl solutions; viscosities of NaCl solutions and self-diffusion data of methane at pressures 1−300 bar (PDF)

■ AUTHOR INFORMATION

Corresponding Authors

Othonas A. Moultos − *Engineering Thermodynamics, Process & Energy Department, Faculty of Mechanical, Maritime and Materials Engineering, Delft University of Technology, Delft 2628CB, The Netherlands;* orcid.org/0000-0001-7477-9684; Email: O.Moultos@tudelft.nl

Thijs J. H. Vlugt − *Engineering Thermodynamics, Process & Energy Department, Faculty of Mechanical, Maritime and Materials Engineering, Delft University of Technology, Delft 2628CB, The Netherlands;* orcid.org/0000-0003-3059-8712; Email: T.J.H.Vlugt@tudelft.nl

Authors

Bin Fang − *School of Mathematics and Physics, China University of Geosciences, Wuhan 430074, China; Engineering Thermodynamics, Process & Energy Department, Faculty of Mechanical, Maritime and Materials Engineering, Delft University of Technology, Delft 2628CB, The Netherlands;* orcid.org/0000-0003-0909-2151

Parsa Habibi − *Engineering Thermodynamics, Process & Energy Department, Faculty of Mechanical, Maritime and Materials Engineering, Delft University of Technology, Delft 2628CB, The Netherlands*

Tao Lü − *School of Automation, China University of Geosciences, Wuhan 430074, China; Hubei Key Laboratory of Advanced Control and Intelligent Automation for Complex Systems, Wuhan 430074, China;* orcid.org/0000-0002-6317-8039

https://doi.org/10.1021/acs.jced.3c00225
J. Chem. Eng. Data 2024, 69, 3330−3346

Fulong Ning − *Faculty of Engineering, China University of Geosciences, Wuhan, Hubei 430074, China; National Center for International Research on Deep Earth Drilling and Resource Development, China University of Geosciences, Wuhan 430074, China;* orcid.org/0000-0003-1236-586X

Complete contact information is available at: https://pubs.acs.org/10.1021/acs.jced.3c00225

Notes

The authors declare no competing financial interest.

■ ACKNOWLEDGMENTS

This work was supported by the National Natural Science Foundation of China (Grants 42206235 and 42225207), the National Key Research and Development Project (No. 2018YFE0126400), and the International Postdoctoral Exchange Fellowship Program (No. PC2021073).

■ REFERENCES

(1) Sloan, E. D.; Koh, C. A. *Clathrate Hydrates of Natural Gases*; CRC Press: Boca Raton, FL, 2007.
(2) Tohidi, B.; Danesh, A.; Todd, A. C.; Burgass, R. W. Hydrate-free zone for synthetic and real reservoir fluids in the presence of saline water. *Chem. Eng. Sci.* **1997**, *52* (19), 3257−3263.
(3) Florusse, L. J.; Peters, C. J.; Schoonman, J.; Hester, K. C.; Koh, C. A.; Dec, S. F.; Marsh, K. N.; Sloan, E. D. Stable low-pressure hydrogen clusters stored in a binary clathrate hydrate. *Science* **2004**, *306* (5695), 469−471.
(4) Bhattacharjee, G.; Kumar, A.; Sakpal, T.; Kumar, R. Carbon Dioxide Sequestration: Influence of Porous Media on Hydrate Formation Kinetics. *ACS Sustainable Chem. Eng.* **2015**, *3* (6), 1205−1214.
(5) Lee, H.; Lee, J. W.; Kim, D. Y.; Park, J.; Seo, Y. T.; Zeng, H.; Moudrakovski, I. L.; Ratcliffe, C. I.; Ripmeester, J. A. Tuning clathrate hydrates for hydrogen storage. *Nature* **2005**, *434* (7034), 743−746.
(6) Babu, P.; Nambiar, A.; He, T. B.; Karimi, I. A.; Lee, J. D.; Englezos, P.; Linga, P. A Review of Clathrate Hydrate Based Desalination To Strengthen Energy-Water Nexus. *ACS Sustainable Chem. Eng.* **2018**, *6* (7), 8093−8107.
(7) Dong, H. S.; Wang, J. Q.; Xie, Z. X.; Wang, B.; Zhang, L. X.; Shi, Q. Potential applications based on the formation and dissociation of gas hydrates. *Renewable & Sustainable Energy Reviews* **2021**, *143*, 110928.
(8) Kumar, A.; Veluswamy, H. P.; Kumar, R.; Linga, P. Direct use of seawater for rapid methane storage via clathrate (sII) hydrates. *Appl. Energy* **2019**, *235*, 21−30.
(9) Liu, G.; He, L.; Fan, Z.; He, Y.; Wu, Z.; Wang, Z. Investigation of gas solubility and its effects on natural gas reserve and production in tight formations. *Fuel* **2021**, *295*, 120507.
(10) Zeron, I. M.; Gonzalez, M. A.; Errani, E.; Vega, C.; Abascal, J. L. F. In Silico" Seawater. *J. Chem. Theory Comput.* **2021**, *17* (3), 1715−1725.
(11) Culberson, O. L.; McKetta, J. J., Jr. Phase Equilibria In Hydrocarbon-Water Systems IV - Vapor-Liquid Equilibrium Constants in the Methane-Water and Ethane-Water Systems. *Journal of Petroleum Technology* **1951**, *3* (11), 297−300.
(12) Chapoy, A. *Phase behaviour in water/hydrocarbon mixtures involved in gas production systems*; École Nationale Supérieure des Mines de Paris, 2004.
(13) Yang, S.; Cho, S.; Lee, H.; Lee, C. Measurement and prediction of phase equilibria for water+ methane in hydrate forming conditions. *Fluid Phase Equilib.* **2001**, *185* (1−2), 53−63.
(14) Lekvam, K.; Bishnoi, P. R. Dissolution of methane in water at low temperatures and intermediate pressures. *Fluid Phase Equilib.* **1997**, *131* (1−2), 297−309.
(15) Crovetto, R.; Fernández-Prini, R.; Japas, M. L. Solubilities of inert gases and methane in H_2O and in D_2O in the temperature range of 300 to 600 K. *J. Chem. Phys.* **1982**, *76* (2), 1077−1086.
(16) Moudgil, B. M.; Somasundaran, P.; Lin, I. J. Automated constant pressure reactor for measuring solubilities of gases in aqueous solutions. *Rev. Sci. Instrum.* **1974**, *45* (3), 406−409.
(17) Ben-Naim, A.; Yaacobi, M. Effects of solutes on the strength of hydrophobic interaction and its temperature dependence. *J. Phys. Chem.* **1974**, *78* (2), 170−175.
(18) Claussen, W.; Polglase, M. Solubilities and structures in aqueous aliphatic hydrocarbon solutions. *J. Am. Chem. Soc.* **1952**, *74* (19), 4817−4819.
(19) Kobayashi, R.; Katz, D. Vapor-liquid equilibria for binary hydrocarbon-water systems. *Industrial Engineering Chemistry* **1953**, *45* (2), 440−446.
(20) Wehe, A.; McKetta, J. Method for determining total hydrocarbons dissolved in water. *Anal. Chem.* **1961**, *33* (2), 291−293.
(21) Gaudette, J.; Servio, P. Measurement of Dissolved Propane in Water in the Presence of Gas Hydrate. *Journal of Chemical & Engineering Data* **2007**, *52* (4), 1449−1451.
(22) Michels, A.; Gerver, J.; Bijl, A. The influence of pressure on the solubility of gases. *Physica* **1936**, *3* (8), 797−808.
(23) Duffy, J. R.; Smith, N. O.; Nagy, B. Solubility of natural gases in aqueous salt solutions—I: Liquidus surfaces in the system CH_4-H_2O-$NaCl_2$-$CaCl_2$ at room temperatures and at pressures below 1000 psia. *Geochim. Cosmochim. Acta* **1961**, *24* (1), 23−31.
(24) O'Sullivan, T. D.; Smith, N. O. Solubility and partial molar volume of nitrogen and methane in water and in aqueous sodium chloride from 50 to 125.deg. and 100 to 600 atm. *J. Phys. Chem.* **1970**, *74* (7), 1460−1466.
(25) Blount, C. W.; Price, L. C.; Wenger, L. M.; Tarullo, M. Methane solubility in aqueous NaCl solutions at elevated temperatures and pressures. In *4th US Gulf Coast Geopressured-Geothermal Energy Conference: Research and Development*; 1979; pp 1225−1260.
(26) Stoessell, R. K.; Byrne, P. A. Salting-out of methane in single-salt solutions at 25°C and below 800 psia. *Geochim. Cosmochim. Acta* **1982**, *46* (8), 1327−1332.
(27) Krader, T.; Franck, E. U. The Ternary Systems H_2O-CH_4-NaCl and H_2O-CH_4-$CaCl_2$ to 800 K and 250 MPa. *Berichte der Bunsengesellschaft für physikalische Chemie* **1987**, *91* (6), 627−634.
(28) Kim, Y.; Lim, B.; Lee, J.; Lee, C. Solubilities of carbon dioxide, methane, and ethane in sodium chloride solution containing gas hydrate. *Journal of Chemical & Engineering Data* **2008**, *53* (6), 1351−1354.
(29) Wilhelm, E.; Battino, R.; Wilcock, R. J. Low-pressure solubility of gases in liquid water. *Chem. Rev.* **1977**, *77* (2), 219−262.
(30) Patel, B. H.; Paricaud, P.; Galindo, A.; Maitland, G. C. Prediction of the Salting-Out Effect of Strong Electrolytes on Water + Alkane Solutions. *Ind. Eng. Chem. Res.* **2003**, *42* (16), 3809−3823.
(31) You, S.-S.; Yoo, K.-P.; Lee, C. S. An approximate nonrandom lattice theory of fluids: General derivation and application to pure fluids. *Fluid Phase Equilib.* **1994**, *93*, 193−213.
(32) Breure, B.; Bottini, S. B.; Witkamp, G.-J.; Peters, C. J. Thermodynamic Modeling of the Phase Behavior of Binary Systems of Ionic Liquids and Carbon Dioxide with the Group Contribution Equation of State. *J. Phys. Chem. B* **2007**, *111* (51), 14265−14270.
(33) Gross, J.; Sadowski, G. Perturbed-Chain SAFT: An Equation of State Based on a Perturbation Theory for Chain Molecules. *Ind. Eng. Chem. Res.* **2001**, *40* (4), 1244−1260.
(34) Docherty, H.; Galindo, A.; Vega, C.; Sanz, E. A potential model for methane in water describing correctly the solubility of the gas and the properties of the methane hydrate. *J. Chem. Phys.* **2006**, *125* (7), No. 074510.
(35) Wasik, D. O.; Polat, H. M.; Ramdin, M.; Moultos, O. A.; Calero, S.; Vlugt, T. J. H. Solubility of CO_2 in Aqueous Formic Acid Solutions and the Effect of NaCl Addition: A Molecular Simulation Study. *J. Phys. Chem. C* **2022**, *126* (45), 19424−19434.
(36) van Rooijen, W. A.; Habibi, P.; Xu, K.; Dey, P.; Vlugt, T. J. H.; Hajibeygi, H.; Moultos, O. A. Interfacial Tensions, Solubilities, and

Transport Properties of the H_2/H_2O/NaCl System: A Molecular Simulation Study. *Journal of Chemical & Engineering Data* **2023**, DOI: 10.1021/acs.jced.2c00707.
(37) Mohammadi, M.-R.; Hadavimoghaddam, F.; Atashrouz, S.; Abedi, A.; Hemmati-Sarapardeh, A.; Mohaddespour, A. Modeling the solubility of light hydrocarbon gases and their mixture in brine with machine learning and equations of state. *Sci. Rep.* **2022**, *12* (1), 14943.
(38) Docherty, H.; Galindo, A.; Sanz, E.; Vega, C. Investigation of the salting out of methane from aqueous electrolyte solutions using computer simulations. *J. Phys. Chem. B* **2007**, *111* (30), 8993−9000.
(39) Prausnitz, J. M.; Lichtenthaler, R. N.; De Azevedo, E. G. *Molecular thermodynamics of fluid-phase equilibria*; Pearson Education: 1998.
(40) Weisenberger, S.; Schumpe, A. Estimation of gas solubilities in salt solutions at temperatures from 273 to 363 K. *AlChE J.* **1996**, *42*, 298−300.
(41) Sun, X.; Mohanty, K. K. Kinetic simulation of methane hydrate formation and dissociation in porous media. *Chem. Eng. Sci.* **2006**, *61* (11), 3476−3495.
(42) Fang, B.; Moultos, O. A.; Lü, T.; Sun, J.; Liu, Z.; Ning, F.; Vlugt, T. J. H. Effects of nanobubbles on methane hydrate dissociation: A molecular simulation study. *Fuel* **2023**, *345*, 128230.
(43) Witherspoon, P. A.; Saraf, D. N. Diffusion of Methane, Ethane, Propane, and n-Butane in Water from 25 to 43°. *J. Phys. Chem.* **1965**, *69* (11), 3752−3755.
(44) Wise, D. L.; Houghton, G. The diffusion coefficients of ten slightly soluble gases in water at 10−60°C. *Chem. Eng. Sci.* **1966**, *21*, 999−1010.
(45) Witherspoon, P. A.; Bonoli, L. Correlation of Diffusion Coefficients for Paraffin, Aromatic, and Cycloparaffin Hydrocarbons in Water. *Industrial & Engineering Chemistry Fundamentals* **1969**, *8* (3), 589−591.
(46) Chen, Y. A.; Chu, C. K.; Chen, Y. P.; Chu, L. S.; Lin, S. T.; Chen, L. J. Measurements of diffusion coefficient of methane in water/brine under high pressure. *Terrestrial, Atmospheric Oceanic Sciences* **2018**, *29* (5), 577.
(47) Pokharel, S.; Aryal, N.; Niraula, B. R.; Subedi, A.; Adhikari, N. P. Transport properties of methane, ethane, propane, and n-butane in water. *J. Phys. Commun.* **2018**, *2* (6), No. 065003.
(48) Yeh, I.-C.; Hummer, G. System-Size Dependence of Diffusion Coefficients and Viscosities from Molecular Dynamics Simulations with Periodic Boundary Conditions. *J. Phys. Chem. B* **2004**, *108* (40), 15873−15879.
(49) Celebi, A. T.; Jamali, S. H.; Bardow, A.; Vlugt, T. J. H.; Moultos, O. A. Finite-size effects of diffusion coefficients computed from molecular dynamics: a review of what we have learned so far. *Mol. Simul.* **2021**, *47* (10−11), 831−845.
(50) Ning, F. L.; Yu, Y. B.; Kjelstrup, S.; Vlugt, T. J. H.; Glavatskiy, K. Mechanical properties of clathrate hydrates: status and perspectives. *Energ Environ. Sci.* **2012**, *5* (5), 6779−6795.
(51) Yuan, T.; Spence, G. D.; Hyndman, R. D.; Minshull, T. A.; Singh, S. C. Seismic velocity studies of a gas hydrate bottom-simulating reflector on the northern Cascadia continental margin: Amplitude modeling and full waveform inversion. *J. Geophys Res-Sol Ea* **1999**, *104* (B1), 1179−1191.
(52) Hester, K.; Huo, Z.; Ballard, A.; Koh, C.; Miller, K.; Sloan, E. Thermal expansivity for sI and sII clathrate hydrates. *J. Phys. Chem. B* **2007**, *111* (30), 8830−8835.
(53) Manakov, A. Y.; Likhacheva, A. Y.; Potemkin, V. A.; Ogienko, A. G.; Kurnosov, A. V.; Ancharov, A. I. J. C. Compressibility of gas hydrates. *ChemPhysChem* **2011**, *12* (13), 2476−2484.
(54) Hester, K. C.; Huo, Z.; Ballard, A. L.; Koh, C. A.; Miller, K. T.; Sloan, E. D. Thermal expansivity for sI and sII clathrate hydrates. *J. Phys. Chem. B* **2007**, *111* (30), 8830−8835.
(55) Ikeda, T.; Mae, S.; Yamamuro, O.; Matsuo, T.; Ikeda, S.; Ibberson, R. M. Distortion of host lattice in clathrate hydrate as a function of guest molecule and temperature. *J. Phys. Chem. A* **2000**, *104* (46), 10623−10630.
(56) Murayama, K.; Takeya, S.; Alavi, S.; Ohmura, R. Anisotropic Lattice Expansion of Structure H Clathrate Hydrates Induced by Help Guest: Experiments and Molecular Dynamics Simulations. *J. Phys. Chem. C* **2014**, *118* (37), 21323−21330.
(57) Takeya, S.; Uchida, T.; Kamata, Y.; Nagao, J.; Kida, M.; Minami, H.; Sakagami, H.; Hachikubo, A.; Takahashi, N.; Shoji, H.; et al. Lattice expansion of clathrate hydrates of methane mixtures and natural gas. *Angew. Chem. Int. Edit* **2005**, *44* (42), 6928−6931.
(58) Takeya, S.; Kida, M.; Minami, H.; Sakagami, H.; Hachikubo, A.; Takahashi, N.; Shoji, H.; Soloviev, V.; Wallmann, K.; Biebow, N.; et al. Structure and thermal expansion of natural gas clathrate hydrates. *Chem. Eng. Sci.* **2006**, *61* (8), 2670−2674.
(59) Udachin, K. A.; Ratcliffe, C. I.; Ripmeester, J. A. Structure, composition, and thermal expansion of CO_2 hydrate from single crystal X-ray diffraction measurements. *J. Phys. Chem. B* **2001**, *105* (19), 4200−4204.
(60) Park, Y.; Choi, Y. N.; Yeon, S. H.; Lee, H. Thermal expansivity of tetrahydrofuran clathrate hydrate with diatomic guest molecules. *J. Phys. Chem. B* **2008**, *112* (23), 6897−6899.
(61) Klapproth, A.; Goreshnik, E.; Staykova, D.; Klein, H.; Kuhs, W. F. Structural studies of gas hydrates. *Can. J. Phys.* **2003**, *81* (1−2), 503−518.
(62) Chazallon, B.; Kuhs, W. F. In situ structural properties of N_2, O_2, and air-clathrates by neutron diffraction. *J. Chem. Phys.* **2002**, *117* (1), 308−320.
(63) Kuhs, W. F.; Chazallon, B.; Radaelli, P. G.; Pauer, F. Cage occupancy and compressibility of deuterated N_2-clathrate hydrate by neutron diffraction. *J. Inclus Phenom Mol.* **1997**, *29* (1), 65−77.
(64) Manakov, A. Y.; Likhacheva, A. Y.; Potemkin, V. A.; Ogienko, A. G.; Kurnosov, A. V.; Ancharov, A. I. Compressibility of Gas Hydrates. *ChemPhysChem* **2011**, *12* (13), 2476−2483.
(65) Waite, W. F.; Stern, L. A.; Kirby, S. H.; Winters, W. J.; Mason, D. H. Simultaneous determination of thermal conductivity, thermal diffusivity and specific heat in sI methane hydrate. *Geophys J. Int.* **2007**, *169* (2), 767−774.
(66) Fang, B.; Ning, F.; Cao, P.; Peng, L.; Wu, J.; Zhang, Z.; Vlugt, T. J. H.; Kjelstrup, S. Modeling thermodynamic properties of propane or tetrahydrofuran mixed with carbon dioxide or methane in structure-II clathrate hydrates. *J. Phys. Chem. C* **2017**, *121* (43), 23911−23925.
(67) Ning, F.; Glavatskiy, K.; Ji, Z.; Kjelstrup, S.; Vlugt, T. J. H. Compressibility, thermal expansion coefficient and heat capacity of CH_4 and CO_2 hydrate mixtures using molecular dynamics simulations. *Phys. Chem. Chem. Phys.* **2015**, *17* (4), 2869−2883.
(68) Abascal, J. L. F.; Vega, C. A general purpose model for the condensed phases of water: TIP4P/2005. *J. Chem. Phys.* **2005**, *123* (23), 234505.
(69) Martin, M. G.; Siepmann, J. I. Transferable Potentials for Phase Equilibria. 1. United-Atom Description of n-Alkanes. *J. Phys. Chem. B* **1998**, *102* (14), 2569−2577.
(70) Zeron, I. M.; Abascal, J. L. F.; Vega, C. A force field of Li^+, Na^+, K^+, Mg^{2+}, Ca^{2+}, Cl^-, and SO_4^{2-} in aqueous solution based on the TIP4P/2005 water model and scaled charges for the ions. *J. Chem. Phys.* **2019**, *151* (13), 134504.
(71) Lennard-Jones, J. E. Cohesion. *Proceedings of the Physical Society* **1931**, *43* (5), 461−482.
(72) Allen, M. P.; Tildesley, D. J. *Computer Simulation of Liquids*; Clarendon Press, Oxford University Press: Oxford, UK; New York, 1987.
(73) Hens, R.; Rahbari, A.; Caro-Ortiz, S.; Dawass, N.; Erdős, M.; Poursaeidesfahani, A.; Salehi, H. S.; Celebi, A. T.; Ramdin, M.; Moultos, O. A.; et al. Brick-CFCMC: Open Source Software for Monte Carlo Simulations of Phase and Reaction Equilibria Using the Continuous Fractional Component Method. *J. Chem. Inf. Model.* **2020**, *60* (6), 2678−2682.
(74) Rahbari, A.; Hens, R.; Ramdin, M.; Moultos, O. A.; Dubbeldam, D.; Vlugt, T. J. H. Recent advances in the continuous fractional component Monte Carlo methodology. *Mol. Simul.* **2021**, *47* (10−11), 804−823.

(75) Shi, W.; Maginn, E. J. Improvement in molecule exchange efficiency in Gibbs ensemble Monte Carlo: Development and implementation of the continuous fractional component move. *J. Comput. Chem.* **2008**, *29* (15), 2520−2530.
(76) Rahbari, A.; Hens, R.; Nikolaidis, I. K.; Poursaeidesfahani, A.; Ramdin, M.; Economou, I. G.; Moultos, O. A.; Dubbeldam, D.; Vlugt, T. J. H. Computation of partial molar properties using continuous fractional component Monte Carlo. *Mol. Phys.* **2018**, *116* (21−22), 3331−3344.
(77) Eric, L.; Marcia, H.; Mark, M. *NIST Standard Reference Database 23: Reference Fluid Thermodynamic and Transport Properties-REFPROP, Version 9.1*; Natl Std. Ref. Data Series (NIST NSRDS); National Institute of Standards and Technology, Gaithersburg, MD, 2013.
(78) Wells, B. A.; Chaffee, A. L. Ewald Summation for Molecular Simulations. *J. Chem. Theory Comput.* **2015**, *11* (8), 3684−3695.
(79) Rouher, O. S.; Barduhn, A. J. Hydrates of iso- and normal butane and their mixtures. *Desalination* **1969**, *6* (1), 57−73.
(80) Takeya, S.; Hachikubo, A. Dissociation kinetics of propane−methane and butane−methane hydrates below the melting point of ice. *Phys. Chem. Chem. Phys.* **2021**, *23* (28), 15003−15009.
(81) Takeuchi, F.; Hiratsuka, M.; Ohmura, R.; Alavi, S.; Sum, A. K.; Yasuoka, K. Water proton configurations in structures I, II, and H clathrate hydrate unit cells. *J. Chem. Phys.* **2013**, *138* (12), 124504.
(82) McMullan, R. K.; Jeffrey, G. A. Polyhedral Clathrate Hydrates. IX. Structure of Ethylene Oxide Hydrate. *J. Chem. Phys.* **1965**, *42* (8), 2725−2732.
(83) Hockney, R. W.; Eastwood, J. W. *Computer simulation using particles*; CRC Press: Boca Raton, FL, 2021.
(84) Papadrakakis, M.; Ghionis, P. Conjugate gradient algorithms in nonlinear structural analysis problems. *Computer methods in applied mechanics engineering* **1986**, *59* (1), 11−27.
(85) Martyna, G. J.; Tobias, D. J.; Klein, M. L. Constant pressure molecular dynamics algorithms. *J. Chem. Phys.* **1994**, *101* (5), 4177−4189.
(86) Grubmüller, H.; Heller, H.; Windemuth, A.; Schulten, K. Generalized Verlet algorithm for efficient molecular dynamics simulations with long-range interactions. *Mol. Simul.* **1991**, *6* (1−3), 121−142.
(87) Jamali, S. H.; Wolff, L.; Becker, T. M.; de Groen, M.; Ramdin, M.; Hartkamp, R.; Bardow, A.; Vlugt, T. J. H.; Moultos, O. A. OCTP: A Tool for On-the-Fly Calculation of Transport Properties of Fluids with the Order-n Algorithm in LAMMPS. *J. Chem. Inf. Model.* **2019**, *59* (4), 1290−1294.
(88) Frenkel, D.; Smit, B. *Understanding molecular simulation: from algorithms to applications*; Elsevier: 2001.
(89) Moultos, O. A.; Zhang, Y.; Tsimpanogiannis, I. N.; Economou, I. G.; Maginn, E. J. System-size corrections for self-diffusion coefficients calculated from molecular dynamics simulations: The case of CO_2, n-alkanes, and poly(ethylene glycol) dimethyl ethers. *J. Chem. Phys.* **2016**, *145* (7), No. 074109.
(90) Kim, K.-S.; Kim, C.; Karniadakis, G. E.; Lee, E. K.; Kozak, J. J. Density-dependent finite system-size effects in equilibrium molecular dynamics estimation of shear viscosity: Hydrodynamic and configurational study. *J. Chem. Phys.* **2019**, *151* (10), 104101.
(91) Jamali, S. H.; Hartkamp, R.; Bardas, C.; Söhl, J.; Vlugt, T. J. H.; Moultos, O. A. Shear Viscosity Computed from the Finite-Size Effects of Self-Diffusivity in Equilibrium Molecular Dynamics. *J. Chem. Theory Comput.* **2018**, *14* (11), 5959−5968.
(92) Kikugawa, G.; Ando, S.; Suzuki, J.; Naruke, Y.; Nakano, T.; Ohara, T. Effect of the computational domain size and shape on the self-diffusion coefficient in a Lennard-Jones liquid. *J. Chem. Phys.* **2015**, *142* (2), No. 024503.
(93) Paschek, D. Temperature dependence of the hydrophobic hydration and interaction of simple solutes: An examination of five popular water models. *J. Chem. Phys.* **2004**, *120* (14), 6674−6690.
(94) Krishnan, C. V.; Friedman, H. L. Model calculations for Setchenow coefficients. *J. Solution Chem.* **1974**, *3* (9), 727−744.
(95) Chen, H.; Yan, K. F.; Chen, Z. Y.; Li, X. S.; Zhang, Y.; Xu, C. G. Exploring Guest−Host Interactions in Gas Hydrates: Insights from Quantum Mechanics. *Energy Fuels* **2021**, *35* (22), 18604−18614.

https://doi.org/10.1021/acs.jced.3c00225
J. Chem. Eng. Data 2024, 69, 3330−3346